Calculation of the Aerodynamic Behavior of the Tilt Rotor Aeroacoustic Model (TRAM) in the DNW

Wayne Johnson

Army/NASA Rotorcraft Division
NASA Ames Research Center
Moffett Field, California

Comparisons of measured and calculated aerodynamic behavior of a tiltrotor model are presented. The test of the Tilt Rotor Aeroacoustic Model (TRAM) with a single, 1/4-scale V-22 rotor in the German-Dutch Wind Tunnel (DNW) provides an extensive set of aeroacoustic, performance, and structural loads data. The calculations were performed using the rotorcraft comprehensive analysis CAMRAD II. Presented are comparisons of measured and calculated performance and airloads for helicopter mode operation, as well as calculated induced and profile power. An aerodynamic and wake model and calculation procedure that reflects the unique geometry and phenomena of tiltrotors has been developed. There are major differences between this model and the corresponding aerodynamic and wake model that has been established for helicopter rotors. In general, good correlation between measured and calculated performance and airloads behavior has been shown. Two aspects of the analysis that clearly need improvement are the stall delay model and the trailed vortex formation model.

Notation·

a	speed of sound
A	rotor disk area, πR^2
c_n	blade section normal force coefficient, $N/(\frac{1}{2}\rho U^2 c)$
c_{ref}	blade reference chord
C_P	rotor power coefficient, $P/\rho(\Omega R)^3 A = Q/\rho(\Omega R)^2 RA$
C_T	rotor thrust coefficient, $T/\rho(\Omega R)^2 A$ (shaft axes)
C_X	rotor propulsive force coefficient, $X/\rho(\Omega R)^2 A$ (wind axes, positive forward)
$M^2 c_n$	blade section normal force coefficient times Mach number squared, $N/(\frac{1}{2}\rho a^2 c)$
M_{tip}	blade tip Mach number, $\Omega R/a$
N	number of blades
N	blade section normal force
r	blade radial station (0 to R)
R	blade radius
P	rotor power, $P = \Omega Q$
q	dynamic pressure, $\frac{1}{2}\rho V^2$
Q	rotor torque
T	rotor thrust (shaft axes)
U	blade section resultant velocity (used for c_n), $U^2 = (\Omega r + V\cos\alpha \sin\psi)^2 + (V\sin\alpha)^2$
X	rotor propulsive force (wind axes, positive forward)
V	wind tunnel speed
α, α_s	rotor shaft angle (positive aft, zero for helicopter mode)
μ	advance ratio, $V/\Omega R$
ρ	air density
σ	rotor solidity, $Nc_{ref}/\pi R$ ($\sigma = 0.105$ for TRAM)
ψ	blade azimuth angle (zero azimuth is downstream)
Ω	rotor rotational speed

·*Presented at the American Helicopter Society 57th Annual Forum, Washington, D.C., May 9–11, 2001.*

Introduction

The tiltrotor aircraft configuration has the potential to revolutionize air transportation by providing an economical combination of vertical take-off and landing

capability with efficient, high-speed cruise flight. To achieve this potential it is necessary to have validated analytical tools that will support future tiltrotor aircraft development. These analytical tools must calculate tiltrotor aeromechanical behavior, including performance, structural loads, vibration, and aeroelastic stability, with an accuracy established by correlation with measured tiltrotor data. For many years such correlation has been performed for helicopter rotors (rotors designed for edgewise flight), but correlation activities for tiltrotors have been limited, in part by the absence of appropriate measured data. The test of the Tilt Rotor Aeroacoustic Model (TRAM) with a single, 1/4-scale V-22 rotor in the German-Dutch Wind Tunnel (DNW) now provides an extensive set of aeroacoustic, performance, and structural loads data.

This report documents correlation between the TRAM DNW measured performance and airloads data and CAMRAD II calculations. CAMRAD II is a modern rotorcraft comprehensive analysis, with advanced models intended for application to tiltrotor aircraft as well as helicopters. Comprehensive analyses have undergone extensive correlation with performance and loads measurements on helicopter rotors. The present paper is part of an initial effort to perform an equally extensive correlation with tiltrotor data. The comparison of measurements and calculations presented here focuses on performance and airloads in helicopter mode operation. The correlation establishes the level of predictive capability achievable with current technology; identifies the limitations of the current aerodynamic and wake models of tiltrotors; and leads to recommendations for research to extend tiltrotor aeromechanics analysis capability.

TRAM DNW Test

The purpose of the Tilt Rotor Aeroacoustic Model (TRAM) experimental project is to provide data necessary to validate tiltrotor performance and aeroacoustic prediction methodologies and to investigate and demonstrate advanced civil tiltrotor technologies. The TRAM activity is a key part of the NASA Short Haul Civil Tiltrotor (SHCT) project. The SHCT project is an element of the Aviation Systems Capacity Initiative within NASA.

In April-May 1998 the TRAM was tested in the isolated rotor configuration at the Large Low-speed Facility of the German-Dutch Wind Tunnels (DNW). A preparatory test was conducted in December 1997. These tests were the first comprehensive aeroacoustic tests for a tiltrotor, including not only noise, performance, and structural loads data, but airload and wake measurements as well. The TRAM can also be tested in a full-span configuration, incorporating both rotors and a fuselage model. The TRAM and the DNW test are described in references 1 to 4.

Figure 1 shows the wind tunnel installation of the TRAM isolated rotor. The DNW is a closed return, atmospheric pressure wind tunnel, with three interchangeable test sections. The TRAM test utilized the 6- by 8-meter open-jet test section, which is in a large anechoic testing hall. In this configuration the tunnel has a maximum airspeed of 85 m/sec.

The rotor tested in the DNW was a 1/4-scale (9.5 ft diameter) model of the right-hand V-22 proprotor. The rotor was tested at a tip Mach number of 0.63 in helicopter mode (because of operational limitations, this was lower than the V-22 nominal tip Mach number of 0.71); and 0.59 in airplane mode (matching the V-22). The rotor and nacelle assembly was attached to an acoustically-treated, isolated rotor test stand through a mechanical pivot (the nacelle conversion axis), as shown in figure 1. The nacelle (but not the spinner) contours model the V-22. The test stand contained the electric motor assembly, and was attached to the DNW sting mount. The conversion angle was manually adjusted, set to 90 deg nacelle angle for helicopter mode and 0 deg nacelle angle for airplane mode testing. As shown in figure 1, the sting was at a nominal angle of 15 deg, so a nacelle angle of 75 deg or –15 deg relative to the sting produced the nacelle angle of 90 deg or 0 deg relative to the horizontal. In helicopter mode or airplane mode (fixed nacelle angle), the rotor shaft angle of attack was set by changing the angle of the sting mount. The DNW sting mount automatically adjusted the vertical position to maintain the hub on the tunnel centerline as shaft angle of attack changed.

TRAM Physical Description

The Tilt Rotor Aeroacoustic Model (TRAM) is a general-purpose test bed for moderate-scale tiltrotor models. TRAM consists of two hardware-interchangeable test rigs: an isolated rotor test stand, and a full-span, dual-rotor model. The contractor team of Micro Craft and McDonnell Douglas Helicopter (now Boeing) had overall responsibility for the TRAM development, under the direction of the Aeromechanics Branch, Army/NASA Rotorcraft Division, NASA Ames Research Center.

The TRAM was designed as a 0.25-scale V-22 tiltrotor aircraft model. The rotor has a diameter of 9.5 ft. Nominal 100% rotor speed is 1588 rpm in helicopter mode (790 ft/sec tip speed, tip Mach number 0.708 at standard conditions) and 1331 rpm in airplane mode (662 ft/sec and 0.593 Mach number). The rotor blades and hub are designed as geometrically and dynamically scaled models

of the V-22 blades. The hub is gimbaled with a constant velocity joint consisting of a spherical bearing and elastomeric torque links. The blade set has both strain-gauged and pressure-instrumented blades. The pressure instrumentation consists of 150 transducers (three different types of Kulite transducers) distributed over two rotor blades.

The TRAM blade assembly consists of the rotor blade, the pitch case, and the yoke or flexbeam. All forces and moments at the root of the rotor blade are transferred through its rigid attachment to the pitch case. The outboard centering bearing (between the pitch case and the outboard end of the yoke) allows only the centrifugal force and flapwise and chordwise shears to be transferred to the yoke. Therefore, the yoke and pitch case serve as dual load paths for the shears, while the torsion, flapwise, and chordwise moments are carried exclusively by the pitch case. Near the inboard end of the yoke, the inboard centering bearing carrier transfers the pitch case shears back into the yoke through the inboard centering bearing, which does not allow the transfer of any moments to the yoke. The resultant loads in the yoke are transferred to the rotor hub through a rigid connection. Both centering bearings are designed so that no moments are transmitted. The inboard bearing is also free to move axially. Blade pitch control moments are applied to the pitch case through a conventional pitch arm, control rod, and swashplate assembly.

The rotor hub assembly transfers the loads from the yoke into the rotor shaft. The rotor hub consists of a gimbal that is free to tilt 8 degrees about the hemispherical retainers, without restoring springs. A series of three elastomeric torque links transfer the torque from the gimballed hub to the non-tilting torque link hub. The nacelle (but not the spinner) contours model the V-22. The nacelle contains a six-component rotor balance and an instrumented (torque and residual thrust) flex-coupling to measure rotor performance (forces and torque). The test stand contains the electric motor assembly. The nacelle angle is manually adjusted between helicopter mode (90 deg) and airplane mode (0 deg).

Reference 5 provides complete details of the TRAM physical description. The sources of the data in reference 5 include the design analysis reports, various subsystem qualification and test reports, CAD data, and NASA measurements. Table 1 presents the principal characteristics of the TRAM. The solidity $\sigma = 0.105$ is the official value (thrust-weighted), used to normalize measured and calculated data in this report. The inboard centering bearing at r/R = 0.0631 is the location of the effective flap and lag hinge, with hinge stiffness provided by the yoke and spindle. Figure 2 shows the blade chord and twist distributions.

The TRAM blade airfoils are the V-22 airfoils designated XN28, XN18, XN12, XN09, at radial stations r/R = 0.2544, 0.50, 0.75, 1.00 respectively. The root fairing has a special airfoil section. The airfoil tables used in the present investigation are those generated during the JVX program in the mid 1980's. The airfoil tables contain data for lift, drag, and moment coefficient as a function of angle-of-attack and Mach number. Reference 6 is the source of these airfoil data. The data are from pressure wind tunnel tests of 6.5 inch chord airfoils, at Reynolds number of approximately Re/M = 15 to 20 million (M is the Mach number). For the root fairing the V-22 cuff airfoil data were used, although the contours of the TRAM root fairing do not match the V-22 because of constraints imposed by the blade pitch case geometry and construction. Also used in the present investigation are the current V-22 airfoil tables (identified as the EMD tables). The differences between the JVX and EMD tables are primarily the lift and drag coefficients at negative angle of attack for the XN09 section, and a new table for the cuff airfoil.

The TRAM blade set consists of both strain-gauged and pressure-instrumented blades. There are 150 pressure transducers distributed over two right-hand rotor blades: primarily at radial stations 0.50, 0.62, 0.82, and 0.96 on blade #1, and at radial stations 0.33, 0.72, 0.90, and 0.98 on blade #2. At the start of the test, 135 of the pressure gages were operational. Chordwise rows of pressure transducers are distributed between two blades in a manner that minimizes the difference in span moment caused by mass distribution effects of the instrumentation wiring and spanwise transducer location. A third blade carries all of the required safety of flight strain gauge instrumentation. The structural design of the TRAM blade is based on a prepreg glass/graphite epoxy hybrid composite. The blade consists of precured spar and skin/core assemblies joined during a bonded assembly stage. Instrumentation wiring packages for measuring pressure or strain are surface mounted into recessed cavities on the blade skin. The strain-gauged and pressure-instrumented blades have nominally identical mass distributions and center-of-gravity locations.

The balance and flex-coupling measure forces and torque. Rotor control positions and gimbal motion are measured. There are redundant measurements for most non-rotating quantities, including balance loads. Five radial stations are instrumented for flap and chord bending moment, and four radial stations for torsion moment. Pitch link force is measured on all three blades. Pitch link loads A, B, and C correspond to blades at 240 deg, 120 deg, and 0 deg relative to the reference azimuth. The blade pressure is measured in chordwise arrays (upper and lower surface) at eight radial stations. Leading edge pressures are

measured at additional stations. These pressure measurements can be integrated chordwise to obtain blade section normal force at seven radial stations (there are too few chordwise points at 98% radius to get section normal force). Reference 3 describes the data reduction process for the blade pressures and section normal force.

Rotorcraft Analysis

The TRAM was analyzed using the rotorcraft comprehensive analysis CAMRAD II. CAMRAD II is an aeromechanical analysis of helicopters and rotorcraft that incorporates a combination of advanced technologies, including multibody dynamics, nonlinear finite elements, and rotorcraft aerodynamics. The trim task finds the equilibrium solution (constant or periodic) for a steady state operating condition, in this case a rotor operating in a wind tunnel. For wind tunnel operation, the thrust and flapping (longitudinal and lateral gimbal tilt) are trimmed to target values. The aerodynamic model includes a wake analysis to calculate the rotor nonuniform induced-velocities, using rigid, prescribed or free wake geometry. The results presented here were all obtained using a free wake. CAMRAD II is described in references 7 to 11. CAMRAD II and similar analyses have undergone extensive correlation with performance and loads measurements on helicopter rotors (see, for example, ref. 9). The present paper is part of an initial effort to perform an equally extensive correlation with tiltrotor data.

Structural Dynamic Model

Figure 3 illustrates the CAMRAD II model of the TRAM. The analytical model has a fixed shaft (no test stand dynamics) and constant rotor rotational speed (no drive train dynamics). The hub has a gimbal joint at the center of rotation, with nominal pitch/gimbal coupling of $\delta_3 = -15$ deg. The true kinematics of the gimbal can be analyzed (either Hook's joint or constant speed), but generally for efficiency a simulated gimbal is used, consisting of a flap hinge at the center of rotation, with harmonics of the gimbal motion at multiples of 3 per-rev suppressed in the trim solution. The pitch link flexibility represents all flexibility of the control system.

The TRAM blade root has a dual load-path, consisting of the pitch case and the yoke/spindle, between the inboard and outboard centering bearings (at r/R = 0.06314 and 0.18024 respectively). A CAMRAD II model of this configuration was developed, with a three degree of freedom angular joint at the outboard centering bearing, and a six degree of freedom (angular then linear) joint at the inboard centering bearing. The inboard linear joint has a large spring in the normal (blade thrust) direction, and a zero axial spring stiffness. However, the pitch case is much stiffer than the yoke and flexbeam, so this dual load-path model is unnecessarily complex. An equivalent model of the kinematics consists of flap, lag, and pitch rotations at the inboard centering bearing, plus elastic bending and torsion of the blade outboard of the pitch case. The yoke and spindle provide spring stiffness for these flap and lag rotations. The CAMRAD II model of the TRAM for the results presented here has a single load-path root. At the inboard centering bearing (r/R = 0.06314) there are flap and lag hinges, followed by the blade pitch rotation. The blade is modelled as rigid inboard of these hinges, and from the hinges to r/R = 0.18024 (the pitch case). The equivalent spring stiffnesses about the flap and lag hinges were determined by matching the calculations to the measured nonrotating blade frequencies and deflections. Additional details of the model are given in reference 12.

The pitch axis is the axis of twist of the blade. The elastic axis is assumed to be coincident with the pitch axis. The blade is represented structurally by four elastic beam elements, with nodes at r/R = 0.195, 0.375, 0.595, 0.795, in addition to nodes at the inboard centering bearing (r/R = 0.06314, location of the flap, lag, and pitch rotations) and the outboard centering bearing (r/R = 0.18024). The CAMRAD II solution for the periodic rotor motion in trim used 10 harmonics of 12 cantilever elastic blade modes plus the gimbal degree of freedom. Performance and airloads calculations were also performed neglecting the elastic blade motion (but retaining the gimbal motion, and usually the motion at the flap and lag hinges).

Aerodynamic Model

The aerodynamic model uses lifting-line theory with a vortex wake calculation of the induced velocity. The blade aerodynamic surfaces are represented by 16 panels, from the root cutout of r/R = 0.10558 to the tip, with panel widths varying from 0.09R inboard to 0.025R at the tip. Midpoints of seven of the aerodynamic panels are aligned with the pressure instrumentation on the TRAM blades, to avoid additional interpolation in the comparison of calculated and measured airloads. The drag coefficients in the airfoil tables are corrected to the lower Reynolds number of the 1/4-scale model, using a factor equal to the Reynolds number ratio to the 1/5-power.

There is evidence that rotational effects on the boundary layer produce a delay of separation on rotor blades, particularly for the inboard sections of tiltrotors and wind turbines (refs. 13 and 14). This stall delay is modelled using input factors K_{sd} to modify the lift and drag coefficients obtained from the airfoil tables:

$$c_l = c_{l\ table} + K_{sdL}\left(c_{l\alpha}(\alpha - \alpha_z) - c_{l\ table}\right)$$

$$c_d = c_{d\ table} + K_{sdD}\left(c_{dz} - c_{d\ table}\right)$$

where $c_{l\alpha}$ is the lift-curve slope, and α_z and c_{dz} are the angle of attack and drag coefficient at zero lift. The equations given by Selig (ref. 14) are used to evaluate the stall delay factors, which depend on the blade chord distribution. The values of K_{sd} used in the TRAM analysis are shown in figure 4.

The CAMRAD II rotor wake analysis uses second-order lifting line theory, and the general free wake geometry described in references 10 and 11. For helicopter mode operation (edgewise flight at moderate speed, μ = 0.125 to 0.200), the high twist of the tiltrotor blades results in negative tip loading over most of the advancing side. Hence the dual-peak model must be used, in which the tip vortex is defined by the negative tip loading (not by the maximum positive bound circulation on the inboard part of the blade). A core radius of 20% mean chord is used for the tip vortex. The positive trailed vorticity inboard of the negative tip loading also rolls up in the analysis, with a core radius of 30% mean chord. To avoid having the rollup model respond to small regions of negative loading, the dual-peak model is only used at azimuths where the negative loading extends inboard at least to 0.945R (there are two aerodynamic panels outboard of this radial station). Two revolutions of wake are used, with calculated free distortion. There is partial entrainment of the trailed vorticity into the tip vortex, such that the final tip vortex strength (achieved after 1/4 revolution of wake age) is 70% of the peak bound circulation on the blade. The distorted wake geometry is calculated for the inboard vorticity as well as for the tip vortices, since inboard rollup is used in the negative tip loading areas. However, distortion of the inboard vorticity is not too important, except when drawing the wake geometry. These wake model features and parameters were determined based on the correlation with measured TRAM performance and airloads, as presented below. The resulting wake model is not the same as the model that has been established for helicopter rotors (refs. 10 and 11).

Work with helicopter rotors has established the importance of rolled-up tip vortices in the calculation of the blade airloading. The resulting blade-vortex interactions are dominant contributors to noise, vibration, and oscillatory structural loads in low speed flight. The tiltrotor wake model used in this report also has a rolled-up tip vortex, although with partial entrainment as described above. In addition, airloads calculated using a wake model with multiple trailed vortex elements are presented here. Bruce Charles of The Boeing Company (Mesa) determined that such a wake model gives good correlation with the measured airloads. The multiple-trailer wake model has a discrete trailed vortex line emanating from each of the aerodynamic panel edges. The calculation of the free wake geometry in CAMRAD II includes the distortion of all of these trailed lines.

Data Reduction and Corrections

The following procedures were used during the DNW test of the TRAM. The nacelle angle was fixed for a particular run. For each data point during a run, the wind tunnel speed, rotor rotational speed, and the rotor shaft angle of attack were set to specified values, and the rotor thrust coefficient C_T set using collective pitch control. Cyclic pitch control was used to achieve zero gimbal tilt (really zero maximum rotating-frame gimbal motion) as indicated on the rotor control console. The rotating-frame gimbal motion was measured and recorded by the data system, so the actual one per-rev gimbal motion (and higher harmonics) is available. Typically the lateral and longitudinal gimbal tilt is less than a few tenths of a degree.

The calculations were performed for specified advance ratio ($V/\Omega R$), tip Mach number, and shaft angle of attack. The analysis trim loop adjusts collective and cyclic to achieve target values of the rotor thrust (C_T/σ) and mean gimbal tilt. The shaft angle of attack values in the analysis correspond to the measured values with wind tunnel wall corrections applied. For comparison of trends with operating condition, involving many measured points, the target thrust is a nominal value and the target gimbal tilt is zero. For comparison with specific data points, the measured thrust and measured one per-rev gimbal tilt are the target trim values for the analysis. Similarly, for trends the operating condition is defined by nominal values of advance ratio, tip Mach number, shaft angle of attack, air density, and temperature; while for specific data points the measured values are used.

All measured quantities were sampled at 64 per-rev, except for the pressure and acoustic measurements, which were sampled at 2048 per-rev. Data were collected for 64 revolutions. The first data sample corresponds to zero azimuth. The results in this report are from a single revolution of data obtained by averaging over the 64 revolutions collected. For performance (loads and power) data, the mean values over this averaged revolution are considered. For structural loads data, the mean and oscillatory (1/2-peak-to-peak) values over the averaged revolution are considered. The time histories of the structural load and airload measurements are corrected for the azimuth shift caused by torque link deflection: $\Delta\psi$ = Q/11620 radians, where Q is the measured shaft torque (ft-lb). Thus for a quantity x measured at azimuth ψ the blade is actually at $\psi - \Delta\psi$: $x_{corrected}(\psi) = x_{measured}(\psi + \Delta\psi)$. This correction is implemented by using direct and inverse harmonic analysis. To eliminate high frequency noise, the airloads data are harmonically analyzed, and 64

harmonics are used to reconstruct the time history (with the $\Delta\psi$ shift) at 256 points in a revolution (reduced from 1024 harmonics representing 2048 samples). All the blade-vortex interaction events in the section normal force data are captured using 64 harmonics.

The balance and flex-coupling measure the rotor forces and torque. The axes of the balance measurements are the shaft axes. The data reduction process converts these loads to engineering units, subtracts weight tares, and subtracts aerodynamic tares. The results include the rotor thrust T (in shaft axes) and torque Q. Then the shaft angle of attack (measured, without wind tunnel wall correction) is used to transform the forces to rotor lift L and propulsive force X, in wind axes. These quantities are used here in rotor coefficient form:

$$C_T/\sigma = T/\rho(\Omega R)^2 A\sigma$$

$$C_X/\sigma = X/\rho(\Omega R)^2 A\sigma$$

$$C_P/\sigma = P/\rho(\Omega R)^3 A\sigma = Q/\rho(\Omega R)^2 RA\sigma$$

where ρ is the air density, ΩR is the tip speed, A is the rotor disk area, and $\sigma = 0.105$ is the official solidity value (thrust-weighted). The power P equals ΩQ. By definition, VX is the rotor parasite power, so

$$C_P - \mu C_X = C_{Pio} = C_{Pi} + C_{Po}$$

is the sum of the induced and profile power ($\mu = V/\Omega R$).

In the calculations it is possible to separately evaluate the induced power and the profile power. The induced power can be presented as the ratio $\kappa = C_{Pi}/C_{Pideal}$, where C_{Pideal} is the ideal power obtained from momentum theory. The profile power can be presented as an equivalent blade drag coefficient, $c_{do} = 8C_{Po}/\sigma$, although in airplane mode this expression does not account for the effect of high axial velocity on the profile power.

Wind Tunnel Wall Correction

The measured balance loads of the TRAM in the DNW are corrected for the influence of the wind tunnel walls, by using the corrected shaft angle of attack and wind axis propulsive force:

$$\Delta\alpha = \delta \; 0.02881 \; \frac{C_L/\sigma}{\mu^2}$$

$$\alpha_{corrected} = \alpha_{uncorrected} + \Delta\alpha$$

$$C_X/\sigma_{corrected} = \cos(\Delta\alpha)\, C_X/\sigma - \sin(\Delta\alpha)\, C_L/\sigma$$

where C_L/σ and C_X/σ are the rotor lift and propulsive force coefficients (rotor coefficient definition, in wind axes), μ is the ratio of wind tunnel speed to rotor tip speed, and $\Delta\alpha$ is the angle of attack correction (positive shaft rearward) in radians. The value of the wall correction constant is $\delta = -0.147$ for the TRAM in the DNW. The correction is thus a decrease in the shaft angle of attack (shaft more forward) relative to the wind, and an increase in the rotor propulsive force. The corresponding correction of the rotor lift is neglected for this test. Reference 12 describes the wind tunnel wall correction in more detail, and shows the influence of this correction on the performance correlation.

Tare Corrections

Aerodynamic tares are subtracted from the measured rotor forces and torque. For helicopter mode, the blades were removed but the root fairings around the pitch cases were retained; and the ends of the root fairings were sealed with foam inserts. The equations for the tare correction of the forces and torque is:

measurement = data – weight tare
– (aero tare – aero weight tare)

For the tares with the root fairings installed, the pitch setting corresponded to 5 deg collective pitch at 75% radius (about 32 deg pitch of the root fairings). From the measured tare data, analytical functions of shaft angle of attack and airspeed (α and dynamic pressure q; only α for the weight tare) are generated by least-squares methods. Then the tares are applied by evaluating these functions at the α and q of the measured data point. The weight tare eliminates the influence of gravity on the balance measurements. Note that the aerodynamic weight tare is obtained with the rotor turning (because it was found that the nonrotating aerodynamic weight tare depended on the hub azimuth). So the aerodynamic tare less the aerodynamic weight tare is zero at zero airspeed (hover).

These tare corrections remove the effects of gravity, the spinner, and (for helicopter mode) the blade root fairings from the measured performance data. The calculated performance (forces and power) does not include the blade weight, and the analysis does not model the spinner. The analysis does include the root fairing, so for helicopter mode it is necessary to apply a tare correction to the calculated performance:

calculation = data – (aero tare – aero tare at q=0)

With these tare corrections, the measured and calculated performance data can be directly compared. The calculations must include the root fairing, since the root fairing does influence the wake and the loading on the rest of the blade. Reference 12 describes the analysis tare correction in more detail, and shows the influence of this correction on the performance correlation.

Airloads Data

The data reduction process for the pressure and airloads measurements is described in reference 3. The pressure coefficient is obtained from the pressure by dividing by

the local section dynamic pressure: $c_p = p/(\frac{1}{2}\rho U^2)$. The section velocity U is

$$U^2 = (\Omega r + V\cos\alpha \sin\psi)^2 + (V\sin\alpha)^2$$

where V is the tunnel speed, α the shaft angle of attack (without wall correction), and ψ the blade azimuth angle (without correction for torque link deflection). It follows that the section normal force coefficient, obtained by integrating the pressure coefficients, is $c_n = N/(\frac{1}{2}\rho U^2 c)$; where c is the local chord. Since the operating conditions of interest in this report do not involve significant stall at the measurement locations, it is more interesting to look at the quantity $M^2 c_n = N/(\frac{1}{2}\rho a^2 c)$. Here M=U/a is the section Mach number:

$$M^2 = \left((\Omega r + V\cos\alpha \sin\psi)^2 + (V\sin\alpha)^2\right)/a^2$$
$$= (M_{tip} r + M_{tun}\cos\alpha \sin\psi)^2 + (M_{tun}\sin\alpha)^2$$

with $M_{tip} = \Omega R/a$ the tip Mach number, and $M_{tun} = V/a$ the tunnel Mach number. The time histories of $M^2 c_n$ presented here include the correction of the azimuth angle for the torque link deflection (applied after using the nominal azimuth ψ to calculate M^2). The section airloads can be integrated to obtain the rotor thrust:

$$T = \int \frac{1}{2}\rho\, a^2 c\, (M^2 c_n)\, dr$$

(dimensional) or

$$C_T = \int \frac{1}{2}\, M_{tip}^2\, (Nc/\pi R)\, (M^2 c_n)\, dr$$

(dimensionless), averaged over the rotor azimuth as well. Trapezoidal integration is used over the seven radial stations where c_n is measured, assuming the load is zero at the root cutout and at the tip. In general the difference between the section normal force N and the shaft axis vertical force that gives the thrust is considered, by including the cosine of the section pitch angle in the integrand. For helicopter mode this difference is not large. A comparison of the rotor thrust measured by the balance with the rotor thrust obtained by integrating the blade pressure measurements shows that the thrust from the airloads is consistently lower than the thrust from the balance, by 15 to 19%. The balance measurement of rotor thrust is considered accurate. The cause of this difference is not known. Examination of the chordwise pressure distributions at the seven radial stations does not suggest any problem.

DNW Test Results

The operating conditions of the TRAM in the DNW covered helicopter mode, airplane mode, and hover. The rotor shaft angle of attack is positive aft, around zero (–14 to +14 deg) for helicopter mode and around –90 deg for airplane mode. The tip Mach number M_{tip} is the ratio of the rotor tip speed to the speed of sound. The advance ratio μ is the ratio of the tunnel speed to the rotor tip speed, regardless of the shaft angle. The helicopter mode test points are for nominal advance ratios of μ = 0.125, 0.150, 0.175, 0.200; nominal thrust coefficients of C_T = 0.009, 0.011, 0.013; at shaft angles from –14 deg to 12 deg. The airplane mode test points are for nominal advance ratios of μ = 0.325, 0.350, 0.375; at shaft angles from –95 deg to –85 deg. Hover tests were conducted in both helicopter mode and airplane mode (shaft angle of 0 and –76 deg respectively, with the tunnel circuit 90% blocked for airplane mode), at thrusts up to approximately C_T/σ = 0.17. Reference 12 provides further details of the TRAM test results from the DNW.

For detailed examination of the airloads and structural loads in helicopter mode forward flight, twelve points were selected. The nominal operation condition is advance ratio $V/\Omega R$ = 0.15, rotor thrust C_T/σ = 0.089 and 0.128, shaft angle of attack from –10 deg (forward) to +10 deg (aft). Table 2 gives the details of the measured operating condition for these twelve points. The corrected shaft angle of attack includes the effect of the wind tunnel walls; the rotor propulsive force C_X/σ is the corrected value. The azimuth correction $\Delta\psi$ accounts for the torque link deflection. The gimbal tilt is obtained from the first harmonics of the measured gimbal deflection. The longitudinal gimbal tilt β_{1c} is positive forward; the lateral gimbal tilt β_{1s} is positive towards the advancing side. For each of the twelve operating conditions examined, airloads data are available for several repeat points (at least three points, as many as eight points). The airloads data from different points at the same operating condition exhibit little difference.

Helicopter Mode Performance

The TRAM helicopter mode performance measured in the DNW is shown in figure 5, in terms of rotor power and propulsive force as a function shaft angle of attack for two rotor thrust values and four advance ratios. Most of the reduction of power as angle of attack increases is accounted for by the parasite power (μC_X), but the equivalent drag still shows a decrease with angle of attack, indicating that the tiltrotor (like the helicopter rotor) becomes more efficient as the propulsive force is reduced. The power increases with thrust, and decreases with advance ratio, as expected at low speed. Most of the variation of the propulsive force with shaft angle of attack and thrust is accounted for by the tilt of the thrust vector with the shaft (αC_T), so the shaft-axis inplane force is a relatively constant drag value. Figure 5 compares the measured helicopter mode performance with calculations using a rigid blade model and the tiltrotor aerodynamic and wake model described above. The calculated power generally matches the measurements well, although the calculated power is too low at low thrust and the middle of

the angle of attack range; and the slope with angle of attack is somewhat too small for $\mu = 0.15$ and high thrust. In addition, the calculated power is somewhat erratic, reflecting the complexity of the wake at these operating conditions. The calculated propulsive force matches the data well, so the differences between measurement and calculation are similar for power and equivalent drag. Both the wind tunnel wall correction and the analysis tare correction are required for best correlation between measured and calculated performance (reference 12). There is little influence of the blade elastic motion on the calculated performance.

The influence of the aerodynamic model on the calculated TRAM helicopter mode performance for $\mu = 0.15$ is examined in figure 6. Without the Reynolds number correction of the drag from the airfoil tables, the calculated power is too low. Without the stall delay model, particularly for the lift, the calculated power is much too high, especially at the higher thrust. Without the stall delay model, the equivalent drag actually increases with angle of attack, because of an increase in the stall at the blade root. The stall delay model is required for accurate calculation of the tiltrotor performance in helicopter mode forward flight. Note however that at low thrust and the middle of the angle of attack range, the induced power is higher, perhaps more realistic, without the stall delay (reflecting the influence on the wake of the lift distribution changes produced by the stall delay model). This implies that a better stall model is needed.

The influence of the wake model on the calculated TRAM helicopter mode performance for $\mu = 0.15$ is examined in figure 7. The wake model for the baseline uses the dual-peak wake model, to accommodate the negative loading on the advancing tip of the blade in helicopter mode; partial entrainment of the trailed vorticity into the tip vortex, such that the final tip vortex strength (achieved after 1/4 revolution of wake age) is 70% of the peak bound circulation on the blade; two revolutions of wake; and a search for the circulation peak only inboard of 0.945R, to avoid having the rollup model respond to small regions of negative loading. Using three revolutions of wake, or unrestricted search for the circulation peak, does not change the calculated performance significantly (not shown in figure 7). However, unrestricted search for the circulation peak results in a calculated induced power that is unreasonably low. Figure 7 shows that using the single-peak wake model increases the calculated power for low thrust, where there is significant negative loading of the blade tip. Using complete entrainment of the tip vortex increases the calculated power for high thrust. For both of these effects, the source of the power increase is a substantial increase of the induced power. The ratio of the tip vortex strength to the peak bound circulation (70% here) is a fixed parameter in this model. It is likely that this ratio actually varies with azimuth.

Through extensive correlation of CAMRAD II calculations with performance and airloads measurements, an aerodynamic and wake model appropriate for most helicopters has been developed (refs. 9 to 11). Figure 8 compares the measured TRAM helicopter mode performance with calculations using this helicopter aerodynamic and wake model, and with calculations using the tiltrotor aerodynamic and wake model documented in this report. The primary differences are that the helicopter model does not include the stall delay, and uses complete entrainment of the tip vortex, three revolutions of wake, and unrestricted search for the circulation peak. For both the tiltrotor and helicopter models, the dual-peak wake model is used, since there is significant negative loading on the rotor blade. At high thrust, the calculated power is much too large with the helicopter model. This power increase is caused by increases both in profile power (without the stall delay) and in the induced power (with complete rollup), as shown in figure 8. Figure 8 also shows that at low thrust the induced power is unreasonably low with the helicopter model (less than the ideal momentum theory value), while the profile power is increased. So at low thrust, the power calculated using the helicopter model shows good correlation with the measured power only because of canceling errors in the calculated induced and profile power. The span loading and wake formation are very different on tiltrotors and helicopters, so it is essential to use model features specific to tiltrotors in order to adequately predict the behavior. The high twist of the tiltrotor blade generally means that the peak bound circulation is not near the tip, implying a partial rollup of the trailed vorticity into the tip vortex. The delay of stall by rotational effects on the inboard blade sections is an aerodynamic phenomenon that should exist on helicopters as well as on tiltrotors. With the low twist of helicopter blades, the angle of attack is not high enough on the inboard part of the blade for the stall delay to have a significant role in redistributing the lift load over the rotor disk.

Figure 8 also shows the performance calculated using the tiltrotor model with the multiple-trailer wake model. It will be shown below that good correlation with measured airloads is obtained using the multiple-trailer wake model. However, the power calculated using the multiple-trailer wake model is significantly larger than measured and the propulsive force is larger, in contrast to the good correlation obtained using the rolled-up wake model. With the multiple-trailer wake model the calculated profile power is lower and the calculated induced power is significantly higher than with the rolled-up wake model. Figure 8 also shows that the erratic behavior exhibited by

results from the rolled-up wake model is absent with the multiple-trailer wake model.

Helicopter Mode Airloads

The blade section airloads (M^2c_n) measured in helicopter mode are presented in figures 9 to 11, for the twelve points at advance ratio $\mu = 0.15$ selected for detailed examination. Each figure shows the airloading as a function of azimuth angle, for all twelve points (six shaft angles and two thrusts), for one of the seven radial stations where the blade pressures are measured. Results are presented for only three radial stations; the results at the other radial stations are similar. Figures 9 to 11 also show the calculated airloads, obtained using the multiple-trailer wake model (with elastic blade). The measured airloads show significant blade-vortex interaction at the tip for all twelve conditions, at both high and low thrust, and at both positive and negative shaft angles. There is a substantial region of negative loading on the advancing blade tip, particularly at low thrust. The calculated and measured airloads compare very well. The measured airloads integrate to a smaller rotor thrust, so the calculated airloads tend to have a larger mean value.

Figures 12 to 17 compare the measured airloads with the calculations using various models, for +6 and –6 deg shaft angle and several radial stations. Each figure presents the airloads calculated using the tiltrotor model with elastic blade and multiple-trailer wake; the tiltrotor model with elastic blade and rolled-up wake; the tiltrotor model with rigid blade and rolled-up wake; and the helicopter model with rigid blade. The measured airloads and the airloads calculated using the multiple-trailer wake compare very well. The measured airloads integrate to a smaller rotor thrust, so the calculated airloads tend to have a larger mean value. The airloads calculated using the other wake models differ significantly from the measurements. The calculations using the rolled-up wake model capture the overall character of the airloads, but there are significant differences in the details. There is little influence of the blade elastic motion on the calculated airloads. Compared to the airloads calculated using the tiltrotor aerodynamic and wake model, the helicopter model produces larger blade-vortex interaction amplitude on the retreating side, smaller blade-vortex interaction amplitude on the advancing side for positive shaft angles, and larger peak airloads on the rotor disk.

Figures 18 to 21 show the distribution of the airloads over the rotor disk (as the blade rotates), for +6 and –6 deg shaft angle. Each figure presents the measured airloads, and the airloads calculated using the tiltrotor model with multiple-trailer wake, the tiltrotor model with rolled-up wake, and the helicopter aerodynamic and wake model. A single scale is used for all plots on all four figures. For comparisons between measurements and calculations, note that the measured airloads integrate to a smaller mean thrust value, and the measurements are only for seven radial stations. The airloads are extrapolated from the last radial station to the tip for both measurements and calculations. The calculations are extrapolated to the root cutout, but the measurements are only plotted to the last radial station available (r = 0.33R). The different blade-vortex interaction and higher peak loading with the helicopter model is evident.

Figures 22 and 23 show the calculated wake geometry for +6 and –6 deg shaft angles, with the rolled-up wake model. The vertical lines on the advancing blade (at an azimuth angle of 105 deg) represent the airloading distribution (M^2c_n), with a common scale on all figures. These figures show the substantial wake distortion and blade-vortex interaction on the advancing side, for both thrust values and all shaft angles; the negative loading on the advancing tip at low thrust; and the general change in the location of the wake relative to the tip-path plane as the shaft angle is varied from negative to positive (from forward to aft). Figures 24 and 25 show the calculated wake geometry with the multiple-trailer wake model, and figures 26 and 27 show the corresponding top views of the wake. The overall, large-scale distortion is similar to that with the rolled-up wake model. Entrainment of the outboard lines into a tip vortex is evident, but requires a substantial wake age to develop.

The wake geometry calculated for the multiple-trailer wake exhibits rollup of the outboard lines into a tip vortex, but because of the spanwise resolution and the absence of viscous effects, a highly concentrated tip vortex is not produced. In contrast, measurements of the TRAM flow field show distinct rolled-up vortex structures, including both positive and negative vortices at low thrust (ref. 15). The vortices produce high-frequency oscillations in the measured airloads (figures 12 to 17), that this multiple-trailer wake model can never produce. In addition, the induced power is larger with the multiple-trailer model, so the performance correlation is not as good as with the rolled-up wake model. It is concluded from these results that while the tiltrotor wake does roll up into concentrated vortices, the rollup process is occurring over a wake age of several revolutions.

Conclusions

Comparisons of measured and calculated aerodynamic behavior of a tiltrotor model have been presented. The measured data are from the test of the Tilt Rotor Aeroacoustic Model (TRAM) with a single, 1/4-scale V-22 rotor in the German-Dutch Wind Tunnel (DNW). The calculations were performed using the rotorcraft comprehensive analysis CAMRAD II. An aerodynamic

and wake model and calculation procedure that reflects the unique geometry and phenomena of tiltrotors has been developed. There are major differences between this model and the corresponding aerodynamic and wake model that has been established for helicopter rotors. The primary differences are that the tiltrotor model includes the stall delay, does not use complete entrainment of the tip vortex, uses two revolutions of wake, and uses a restricted search for the circulation peak. Using this tiltrotor model, good correlation has been shown between measured and calculated performance and airloads in helicopter mode.

For computation of performance In helicopter mode, important model features are the stall delay, the Reynolds number correction, the dual-peak wake model with restricted search for the circulation peak, the wake extent, and the tip vortex formation. Good correlation of measured and calculated performance is achieved, when the wind tunnel wall correction of the measurements and an analysis tare correction are used. The helicopter aerodynamic and wake model does not give adequate performance calculations. The measured airloads and the airloads calculated using the multiple-trailer wake compare very well. However, the multiple-trailer wake does not produce the rolled-up vortex structures observed in the TRAM flow field measurements and implied by the measured high frequency airload variations. In addition, the induced power is larger with the multiple-trailer model, so the performance correlation is not as good as with the rolled-up wake model. The good airloads correlation using the multiple-trailer wake model implies that while the tiltrotor wake does roll up into concentrated vortices, the rollup process is occurring over a wake age of several revolutions.

Two aspects of the analysis that clearly need improvement are the stall delay model and the trailed vortex formation model. These features represent specific physical aspects of rotor aerodynamics, that are described directly, but quite simply, in the aerodynamic and wake model of the analysis. One result of the correlation is to establish values of the parameters that define these features in CAMRAD II. The more general results of the correlation are to establish the key importance of these features for tiltrotor aeromechanics behavior, and the need for improved models. A first-principles solution for rotor aerodynamics is the long term goal. Until that is available, more accurate and more general models of the stall delay and the trailed vortex formation are needed. Acquisition of additional detailed aerodynamic measurements will be needed to support such model development.

Acknowledgments

The experimental results in this paper were derived from research performed under the auspices of the Tilt Rotor Aeroacoustic Model (TRAM) project and the NASA Short Haul Civil Tiltrotor (SHCT) project. The TRAM and SHCT projects are led at NASA Ames Research Center by the Army/NASA Rotorcraft Division and the Advanced Tiltrotor Technology Project Office, respectively. Other major funding partners and research participants in the experimental research effort were the U.S. Army Aeroflightdynamics Directorate (AFDD) located at Ames, the Acoustics Division of NASA Langley Research Center, and The Boeing Company (Mesa). In addition, the outstanding support provided by the German-Dutch Wind Tunnel (DNW) staff during the execution of the wind tunnel test was crucial to the success of the test.

References

1) Young, L.A. "Tilt Rotor Aeroacoustic Model (TRAM): A New Rotorcraft Research Facility." Heli Japan 98: AHS International Meeting on Advanced Rotorcraft Technology and Disaster Relief, April 21–23, 1998, Nagarafukumitsu, Gifu, Japan.

2) Young, L.A.; Booth, E.R., Jr.; Yamauchi, G.K.; Botha, G.; and Dawson, S. "Overview of the Testing of a Small–Scale Proprotor." AHS International 55th Annual Forum Proceedings, Montreal, Canada, May 1999.

3) Swanson, S.M.; McCluer, M.S.; Yamauchi, G.K.; and Swanson, A.A. "Airloads Measurements from a 1/4–Scale Tiltrotor Wind Tunnel Test." 25th European Rotorcraft Forum, Rome, Italy, September 1999.

4) Johnson, J.L., and Young, L.A. "Tilt Rotor Aeroacoustic Model Project." Confederation of European Aerospace Societies (CEAS), Forum on Aeroacoustics of Rotorcraft and Propellers, Rome, Italy, June 1999.

5) Ames Research Center. "TRAM Physical Description." NASA Report (to be published).

6) Jenks, M.D., and Narramore, J.C. "Final Report for the 2–D Test of the Model 901 Rotor and Wing Airfoils (BSWT 592)," Boeing Report D901–99065–1, June 1984.

7) Johnson, W. "CAMRAD II, Comprehensive Analytical Model of Rotorcraft Aerodynamics and Dynamics." Johnson Aeronautics, Palo Alto, California, 1992–1999.

8) Johnson, W. "Technology Drivers in the Development of CAMRAD II." American Helicopter Society Aeromechanics Specialists Conference, San Francisco, California, January 1994.

9) Johnson, W. "Rotorcraft Aeromechanics Applications of a Comprehensive Analysis." Heli Japan 98: AHS

International Meeting on Advanced Rotorcraft Technology and Disaster Relief, April 21–23, 1998.

10) Johnson, W. "A General Free Wake Geometry Calculation for Wings and Rotors." American Helicopter Society 51st Annual Forum Proceedings, Fort Worth, Texas, May 1995.

11) Johnson, W. "Rotorcraft Aerodynamics Models for a Comprehensive Analysis." AHS International 54th Annual Forum Proceedings, Washington, D.C., May 1998.

12) Johnson, W. "Calculation of Tilt Rotor Aeroacoustic Model (TRAM DNW) Performance, Airloads, and Structural Loads." American Helicopter Society Aeromechanics Specialists' Meeting, Atlanta, Georgia, November 2000.

13) Corrigan, J.J., and Schillings, J.J. "Empirical Model for Stall Delay Due to Rotation." American Helicopter Society Aeromechanics Specialists Conference, San Francisco, California, January 1994.

14) Du, Z., and Selig, M.S. "A 3–D Stall–Delay Model for Horizontal Axis Wind Turbine Performance Prediction." AIAA Paper 98–0021, January 1998.

15) Yamauchi, G.K.; Burley, C.L.; Mercker, E.; Pengel, K; and JanakiRam, R. "Flow Measurements of an Isolated Model Tilt Rotor." AHS International 55th Annual Forum Proceedings, Montreal, Canada, May 1999.

Table 1. Principal physical characteristics of the TRAM model.

gimballed hub, trailing pitch link	
blade radius R	4.75 ft
solidity σ (thrust weighted)	0.105
number of blades	3
100% rpm, helicopter	Ω = 1588 rpm
	ΩR = 789.90
	M_{tip} = 0.708
100% rpm, airplane	Ω = 1331 rpm
	ΩR = 662.06
	M_{tip} = 0.593
airfoil sections	XN28, XN18,
	XN12, XN09
precone	2 deg
nominal pitch flap coupling, δ_3	–15 deg

Table 2. Measured operating condition of helicopter mode points selected for detailed examination.

$V/\Omega R = 0.15,\ C_T/\sigma = 0.089$						
nominal shaft angle	–10	–6	–2	2	6	10
run	607	605	605	605	603	603
point	13	231	122	10	7	72
advance ratio, $V/\Omega R$	.1509	.1506	.1509	.1502	.1495	.1506
rotor thrust, C_T/σ	.08814	.08792	.08831	.08895	.08839	.08949
shaft angle of attack	–9.99	–6.00	–2.03	1.99	5.94	9.95
corrected shaft angle of attack	–10.92	–6.94	–2.97	1.04	4.98	9.02
tip Mach number, M_{tip}	.6278	.6248	.6259	.6281	.6294	.6271
air density, ρ	.002334	.002326	.002336	.002354	.002373	.002356
air temperature (deg F)	59.69	64.37	62.62	59.20	57.98	61.55
azimuth correction, $\Delta\psi$	1.48	1.30	1.11	.94	.75	.53
rotor power, C_P/σ	.007386	.006516	.005567	.004656	.003683	.002603
rotor propulsive force, C_X/σ	.01382	.00809	.00191	–.00480	–.01091	–.01628
longitudinal gimbal tilt, β_{1c}	–.04	.07	.09	.03	–.14	–.30
lateral gimbal tilt, β_{1s}	–.08	–.09	.16	.10	–.13	–.33
missing c_n	.96R				.82 R	.82 R
missing flap moment	.365 R	.365 R	.365 R	.365 R	.365 R	.365 R
missing torsion moment	.76 R	.76 R				

$V/\Omega R = 0.15,\ C_T/\sigma = 0.128$						
nominal shaft angle	–10	–6	–2	2	6	10
run	607	605	605	605	603	603
point	68	252	177	68	13	39
advance ratio, $V/\Omega R$	.1506	.1503	.1500	.1512	.1504	.1501
rotor thrust, C_T/σ	.12679	.12619	.12371	.12665	.12662	.12625
shaft angle of attack	–9.98	–5.99	–2.10	1.93	5.95	10.03
corrected shaft angle of attack	–11.32	–7.34	–3.43	.59	4.60	8.69
tip Mach number, M_{tip}	.6264	.6247	.6254	.6266	.6290	.6280
air density, ρ	.002325	.002325	.002330	.002342	.002369	.002361
air temperature (deg F)	61.89	64.64	63.72	61.67	58.90	60.57
azimuth correction, $\Delta\psi$	2.47	2.25	1.92	1.69	1.37	1.02
rotor power, C_P/σ	.012392	.011290	.009617	.008402	.006704	.005002
rotor propulsive force, C_X/σ	.02137	.01239	.00455	–.00377	–.01364	–.02190
longitudinal gimbal tilt, β_{1c}	.06	.26	.09	.10	.22	.23
lateral gimbal tilt, β_{1s}	–.03	.01	.00	.09	.31	.26
missing c_n	.96R				.82 R	.82 R
missing flap moment	.365 R	.365 R	.365 R	.365 R	.365 R	.365 R
missing torsion moment	.76 R	.76 R				

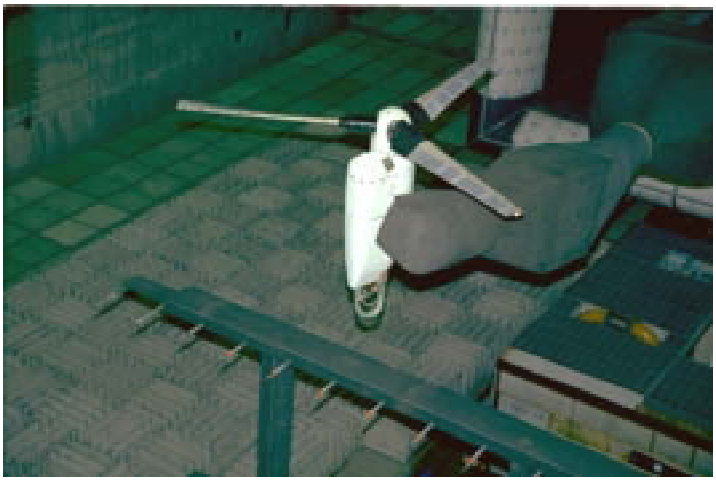

Figure 1. Tilt Rotor Aeroacoustic Model in the German-Dutch Wind Tunnel (TRAM DNW).

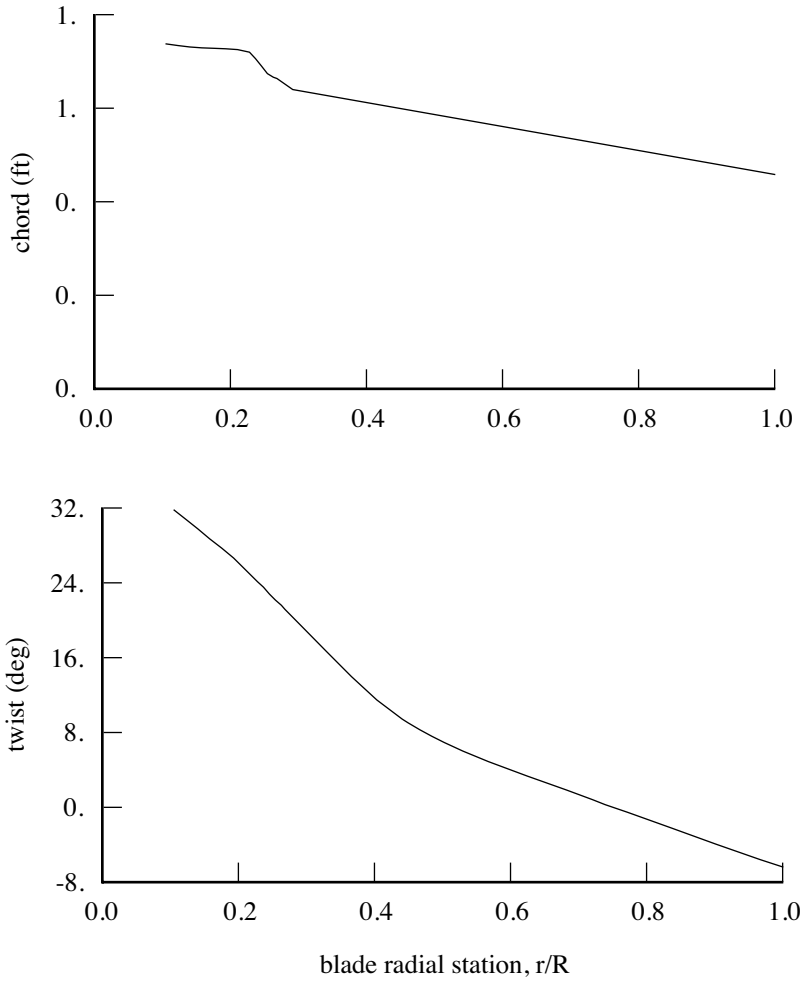

Figure 2. TRAM chord and twist distributions.

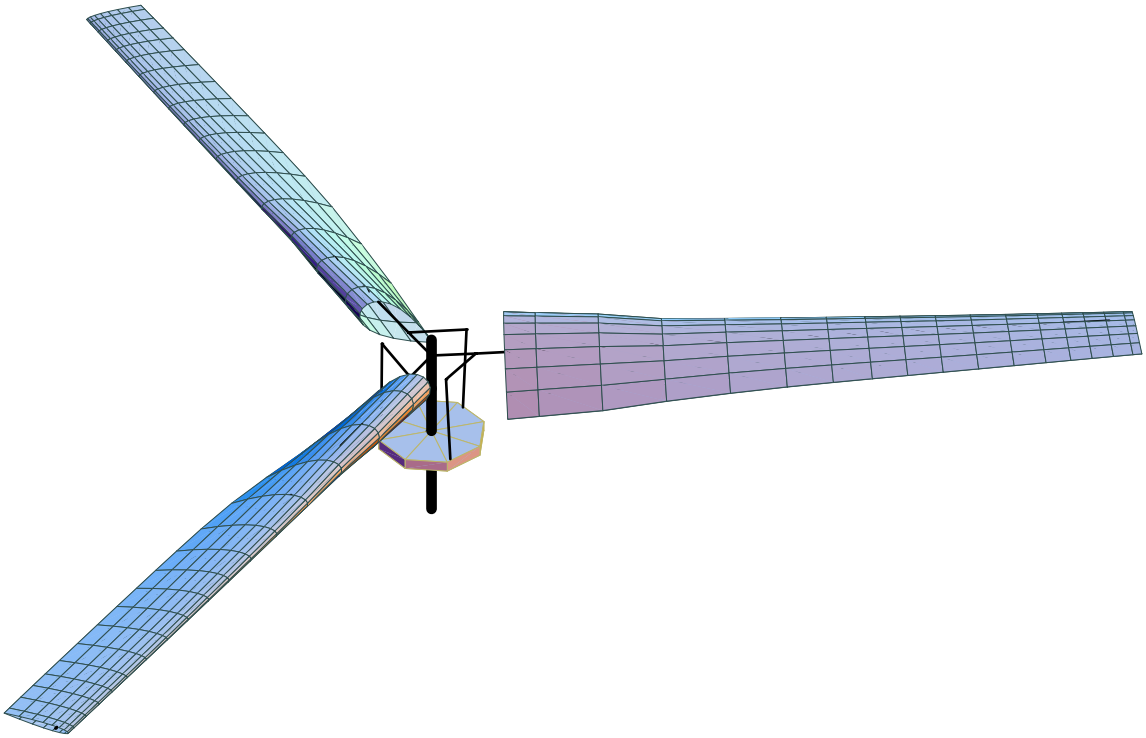

Figure 3. CAMRAD II model of TRAM.

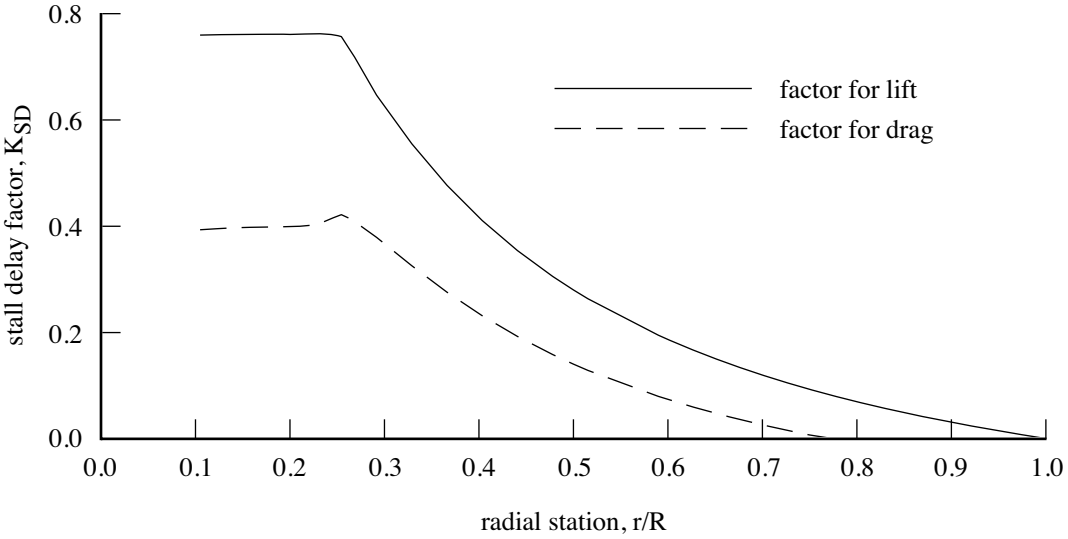

Figure 4. Stall delay factor for TRAM blade.

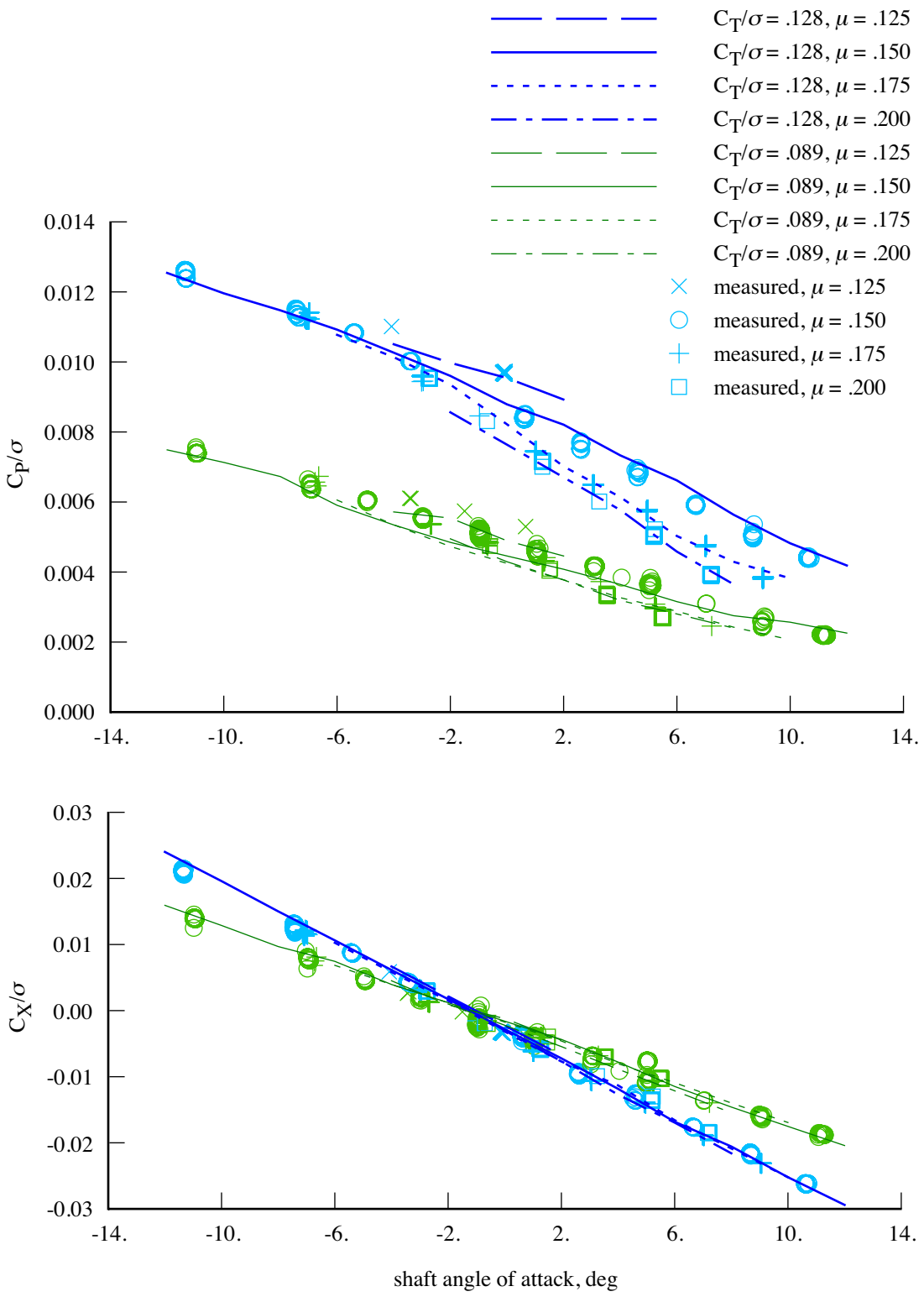

Figure 5. Measured and calculated TRAM helicopter mode performance (rigid blade model).

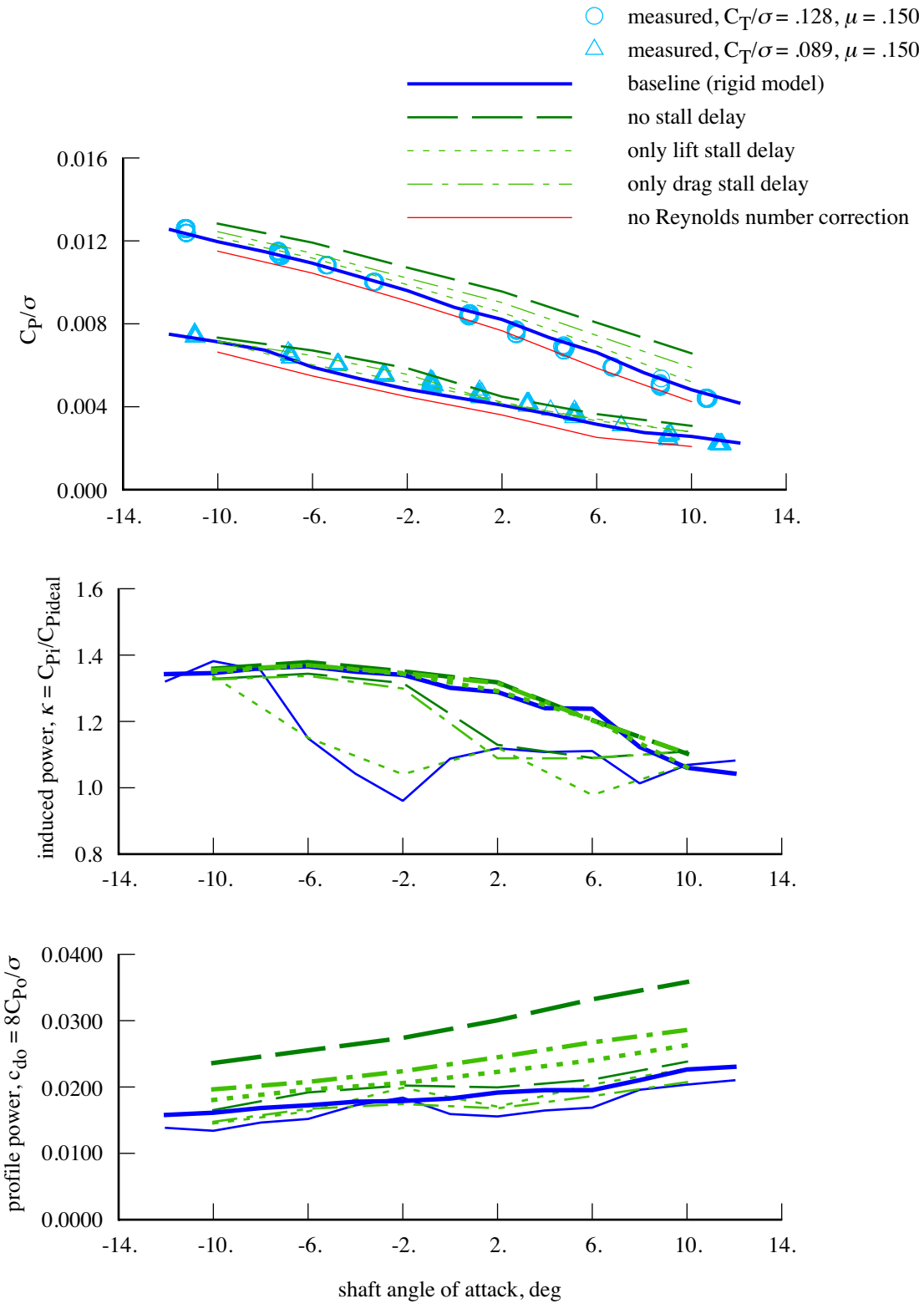

Figure 6. Influence of aerodynamic model on calculated TRAM helicopter mode performance ($\mu = 0.15$; in lower two figures, heavy line $C_T/\sigma = 0.128$, thin line $C_T/\sigma = 0.089$).

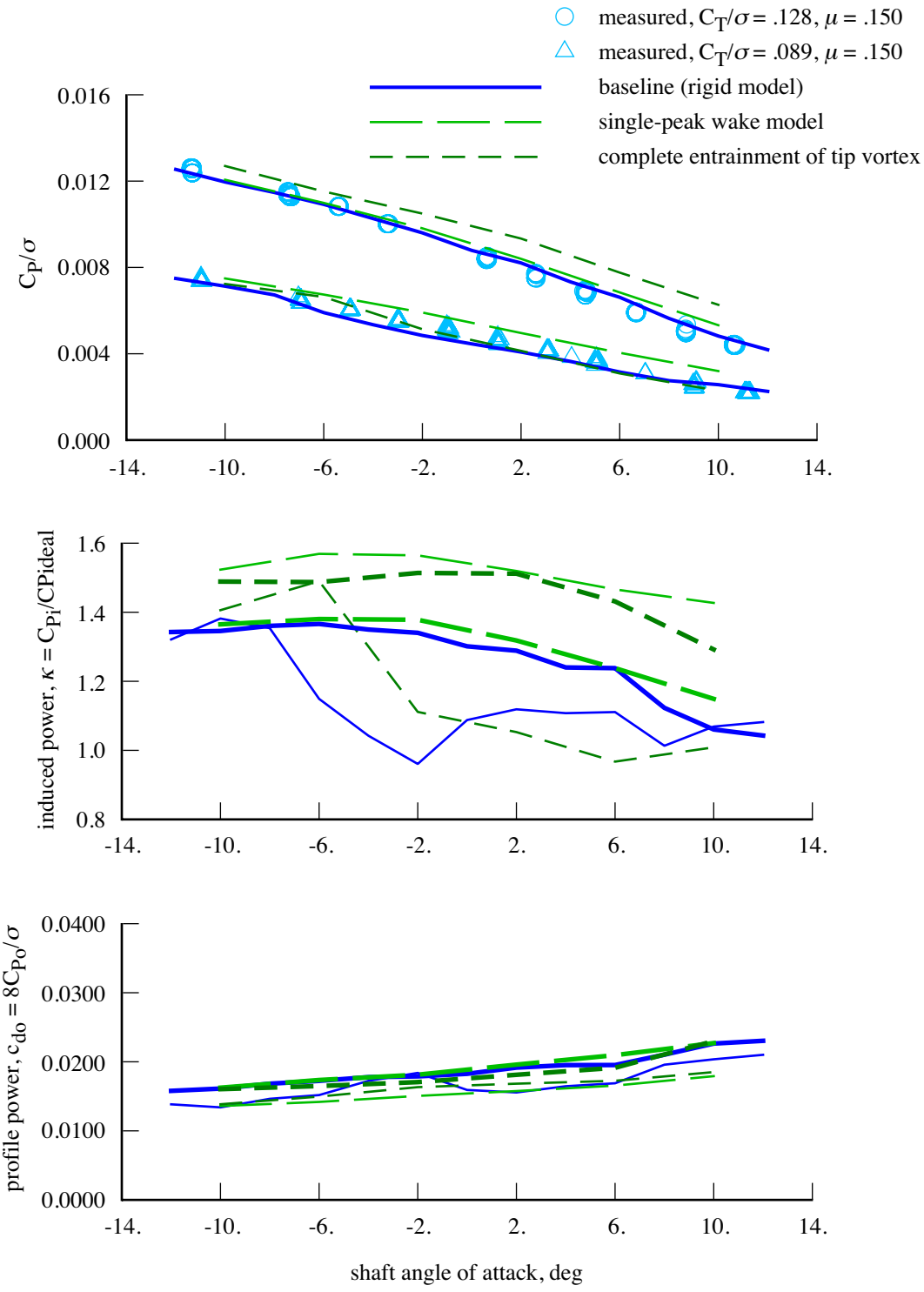

Figure 7. Influence of wake model on calculated TRAM helicopter mode performance ($\mu = 0.15$; in lower two figures, heavy line $C_T/\sigma = 0.128$, thin line $C_T/\sigma = 0.089$).

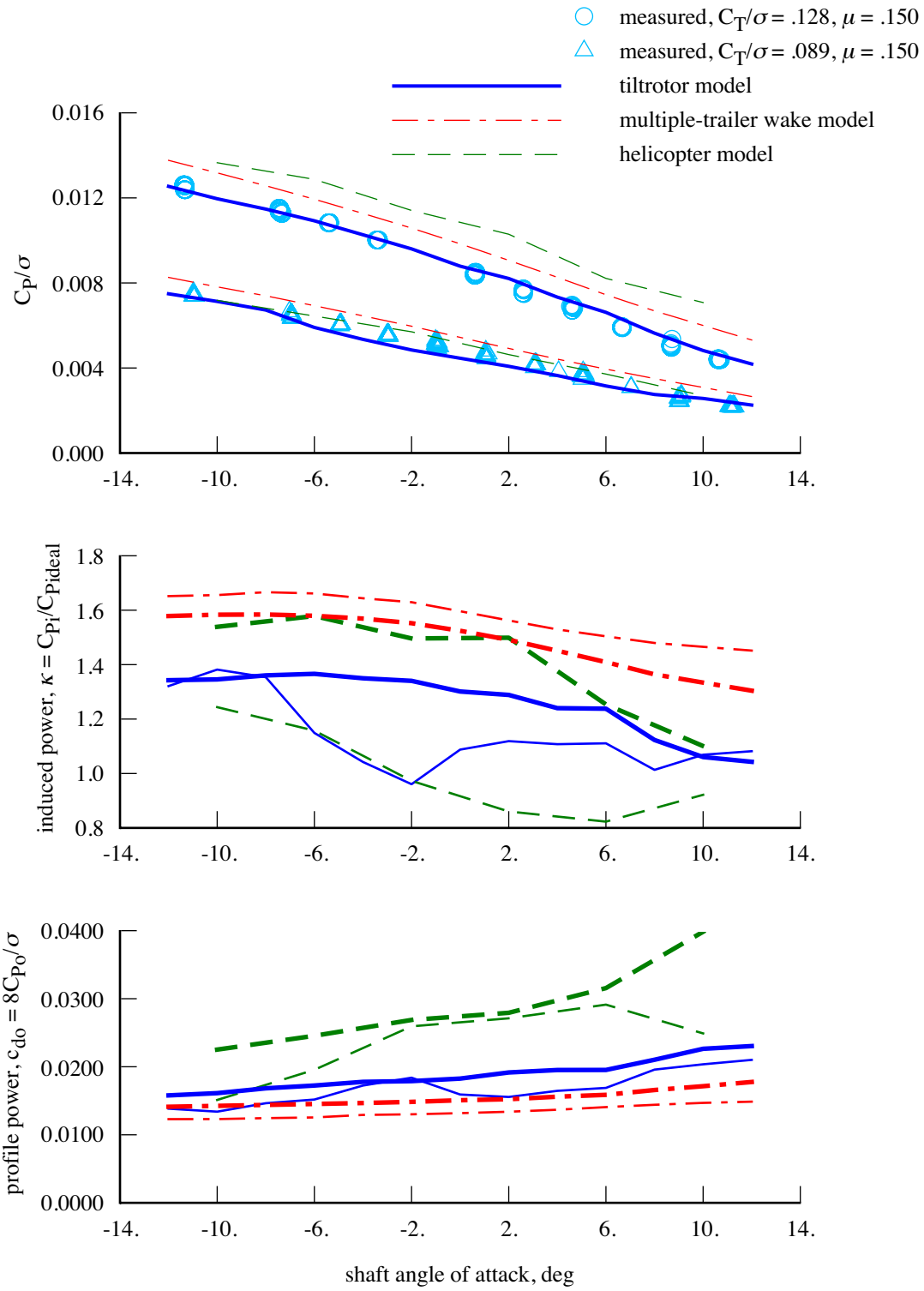

Figure 8. TRAM helicopter mode performance calculated using tiltrotor and helicopter aerodynamic and wake models ($\mu = 0.15$; in lower two figures, heavy line $C_T/\sigma = 0.128$, thin line $C_T/\sigma = 0.089$).

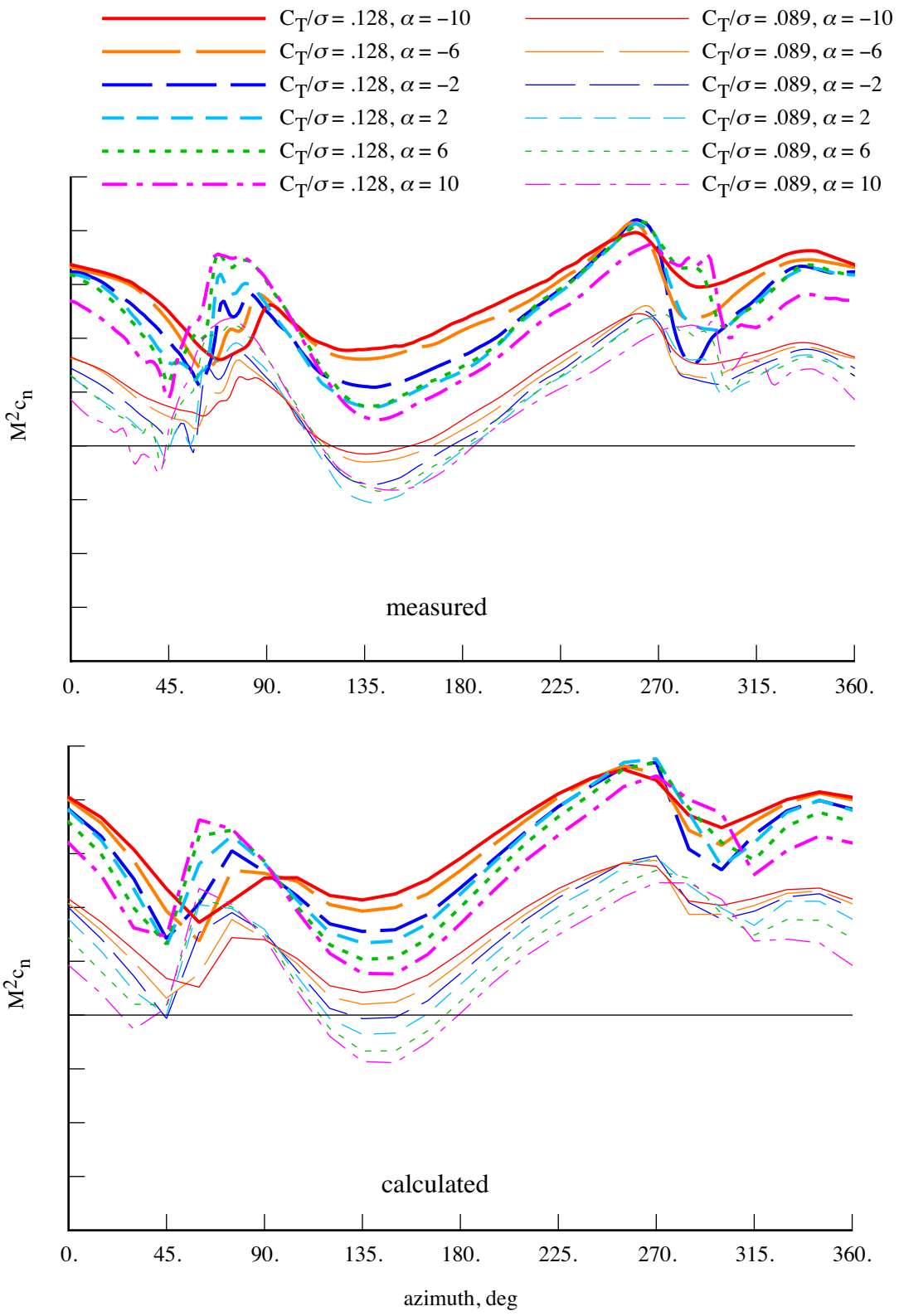

Figure 9. Measured and calculated TRAM helicopter mode airloads ($\mu = 0.15$).
Calculations using tiltrotor model with multiple-trailer wake model. Radial station r = 0.90R.

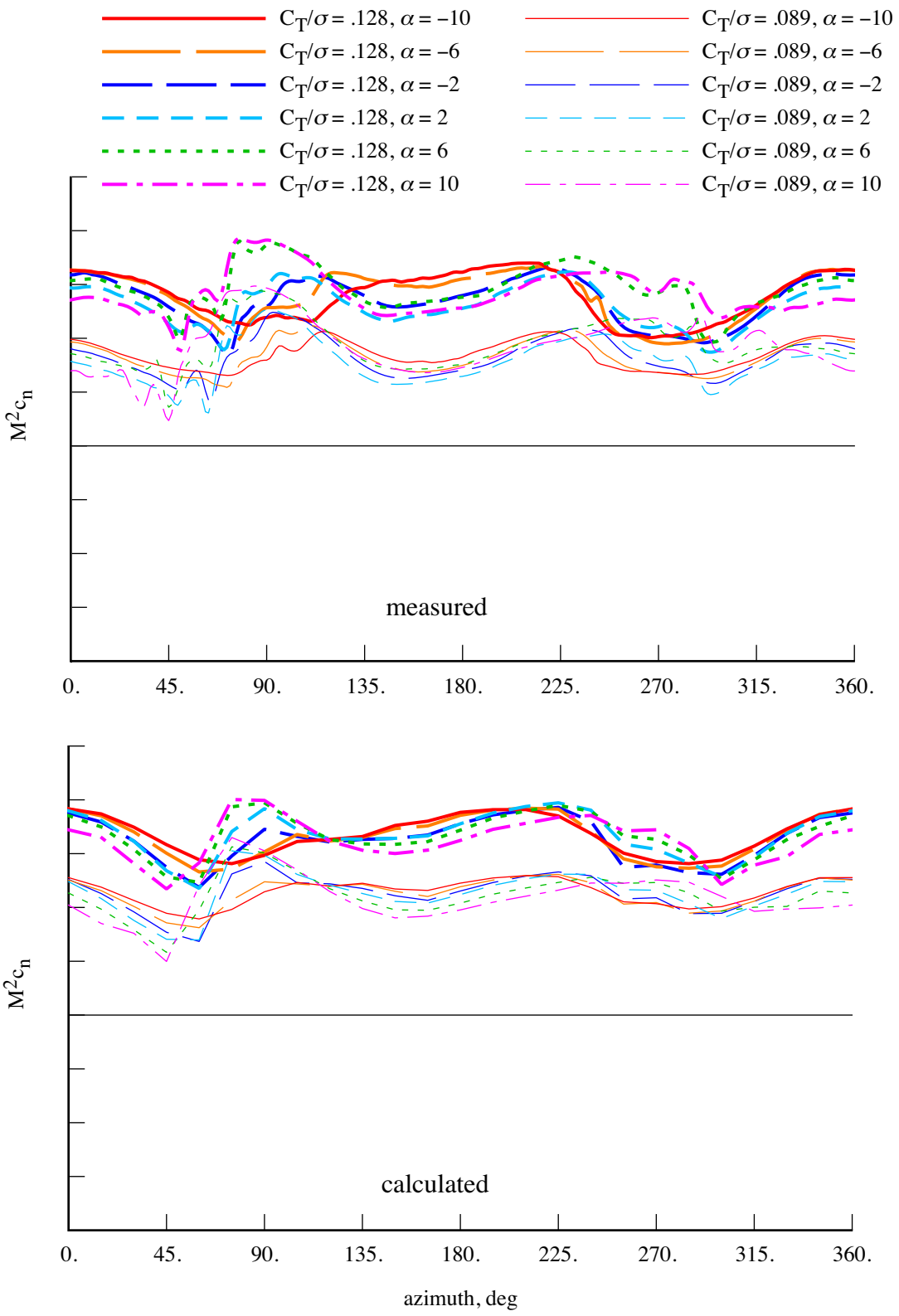

Figure 10. Measured and calculated TRAM helicopter mode airloads ($\mu = 0.15$).
Calculations using tiltrotor model with multiple-trailer wake model. Radial station r = 0.72R.

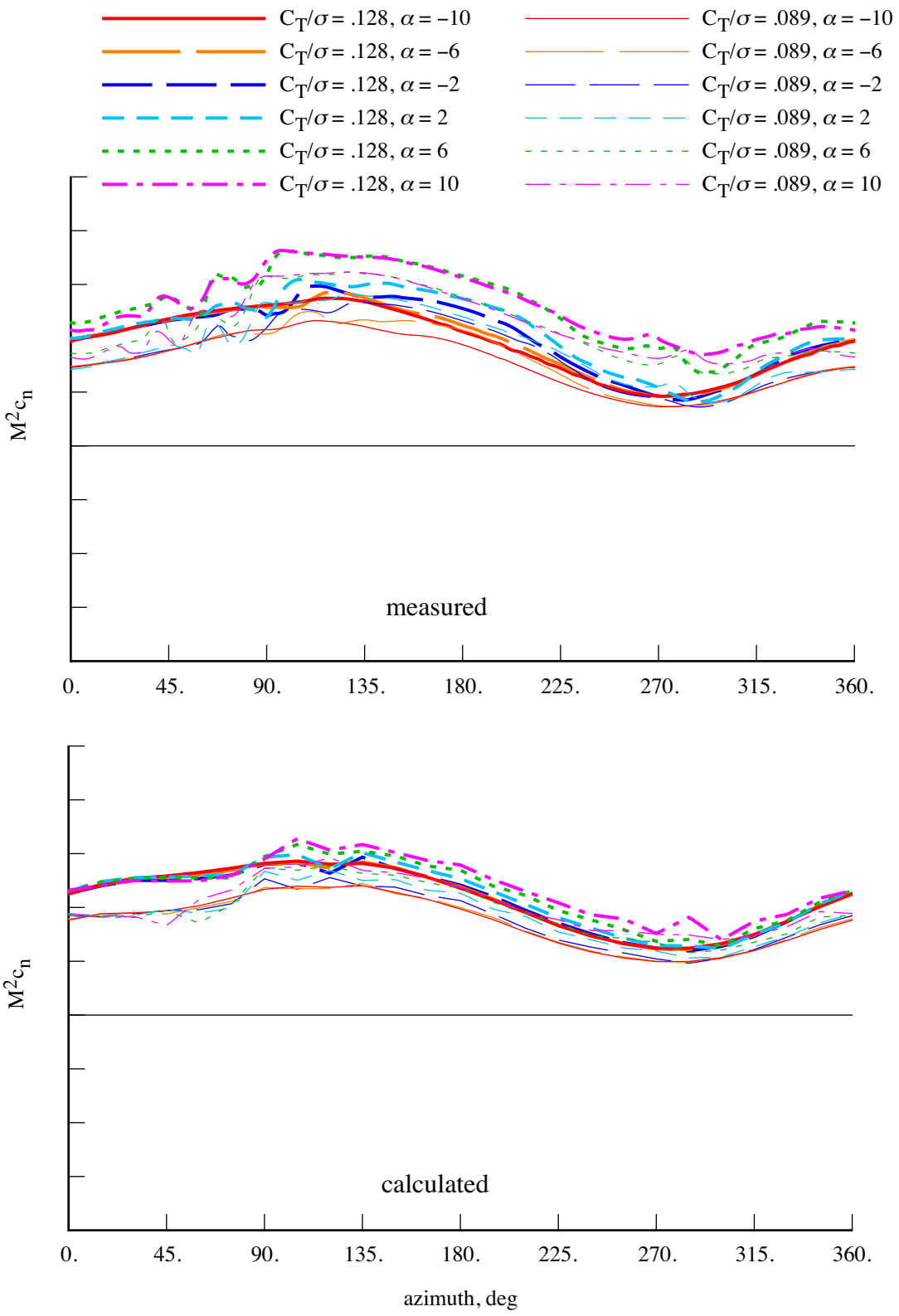

Figure 11. Measured and calculated TRAM helicopter mode airloads ($\mu = 0.15$).
Calculations using tiltrotor model with multiple-trailer wake model. Radial station r = 0.50R.

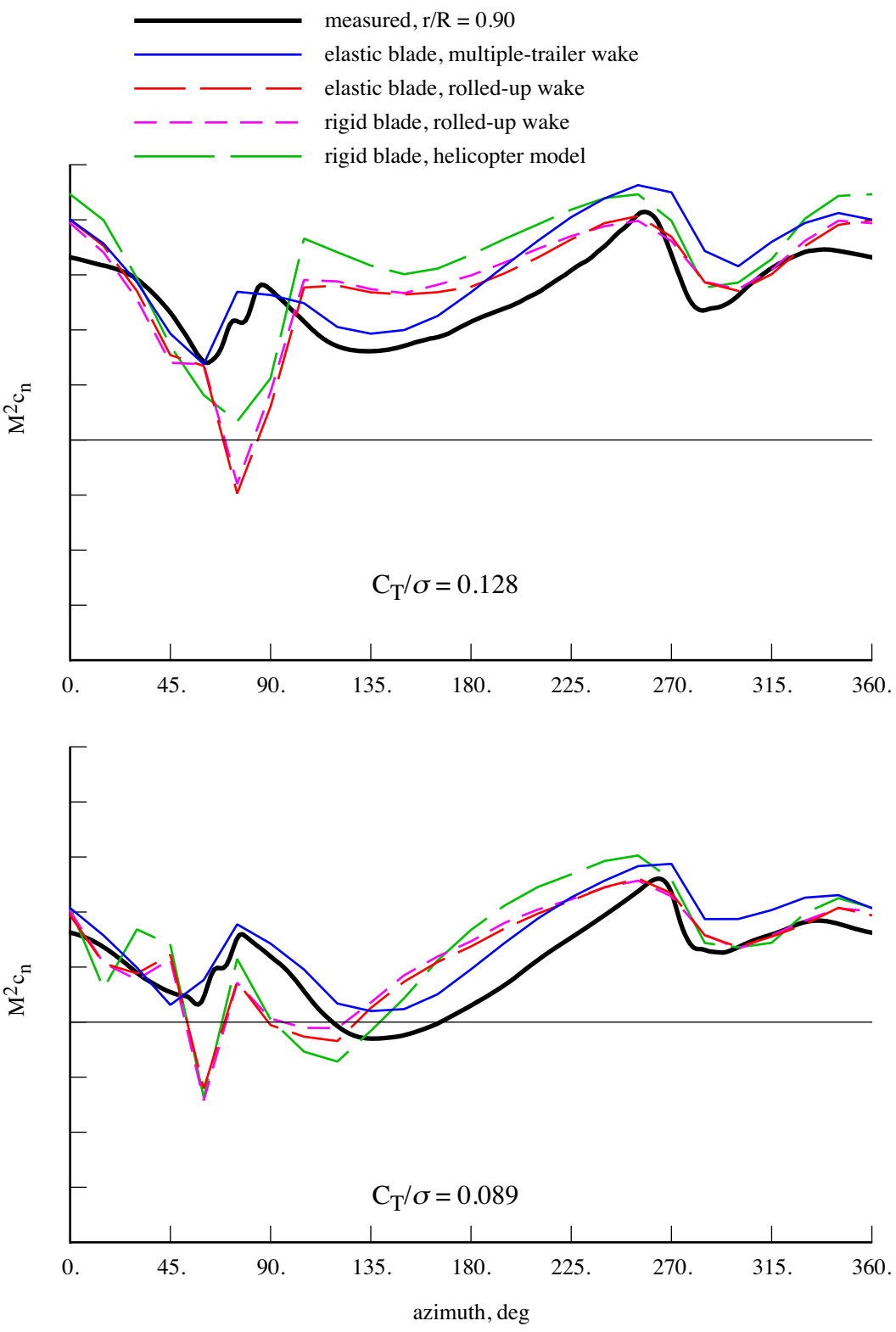

Figure 12. Measured and calculated TRAM helicopter mode airloads for μ = 0.15 and α_s = −6; radial station r = 0.90R.

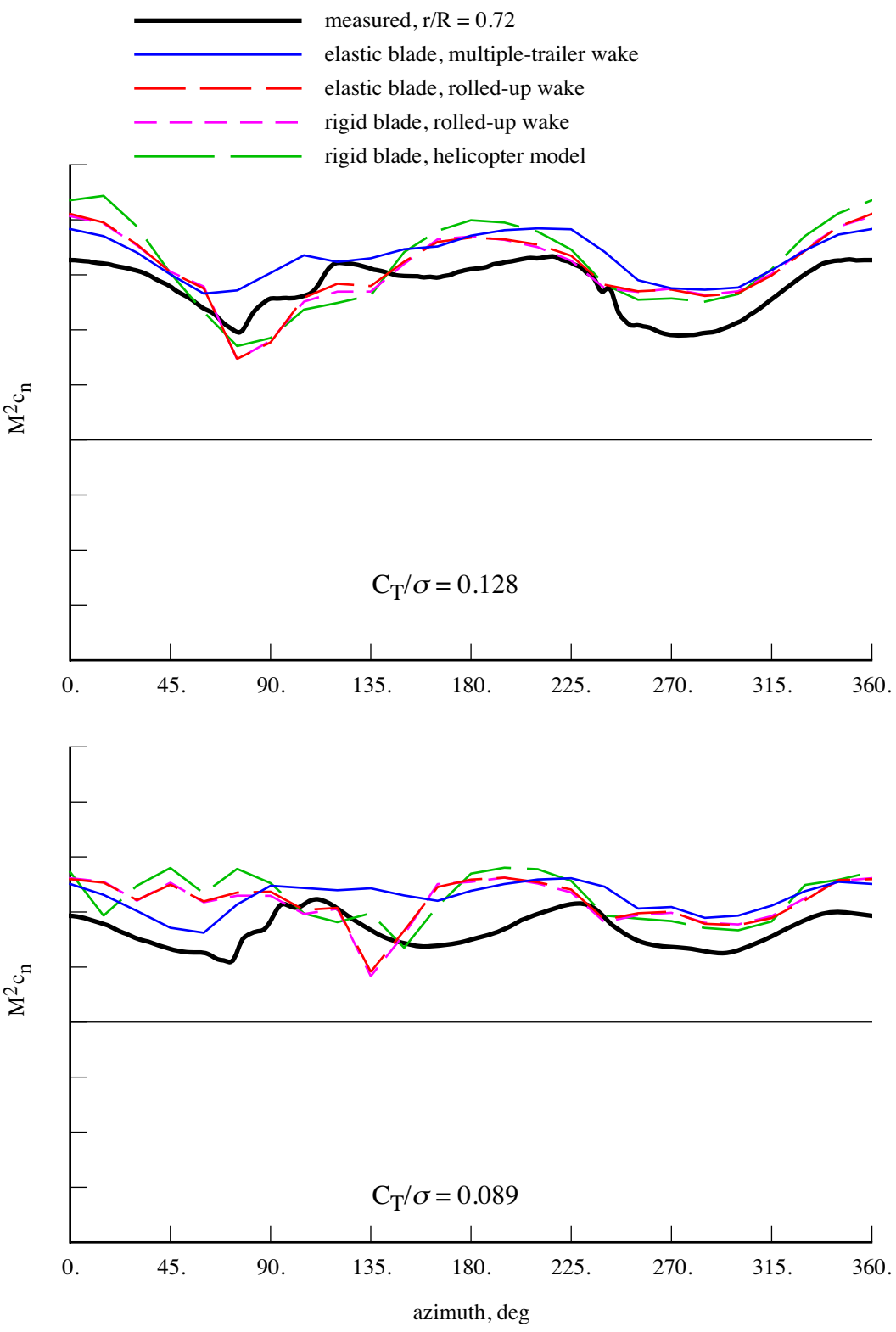

Figure 13. Measured and calculated TRAM helicopter mode airloads for μ = 0.15 and α_s = −6; radial station r = 0.72R.

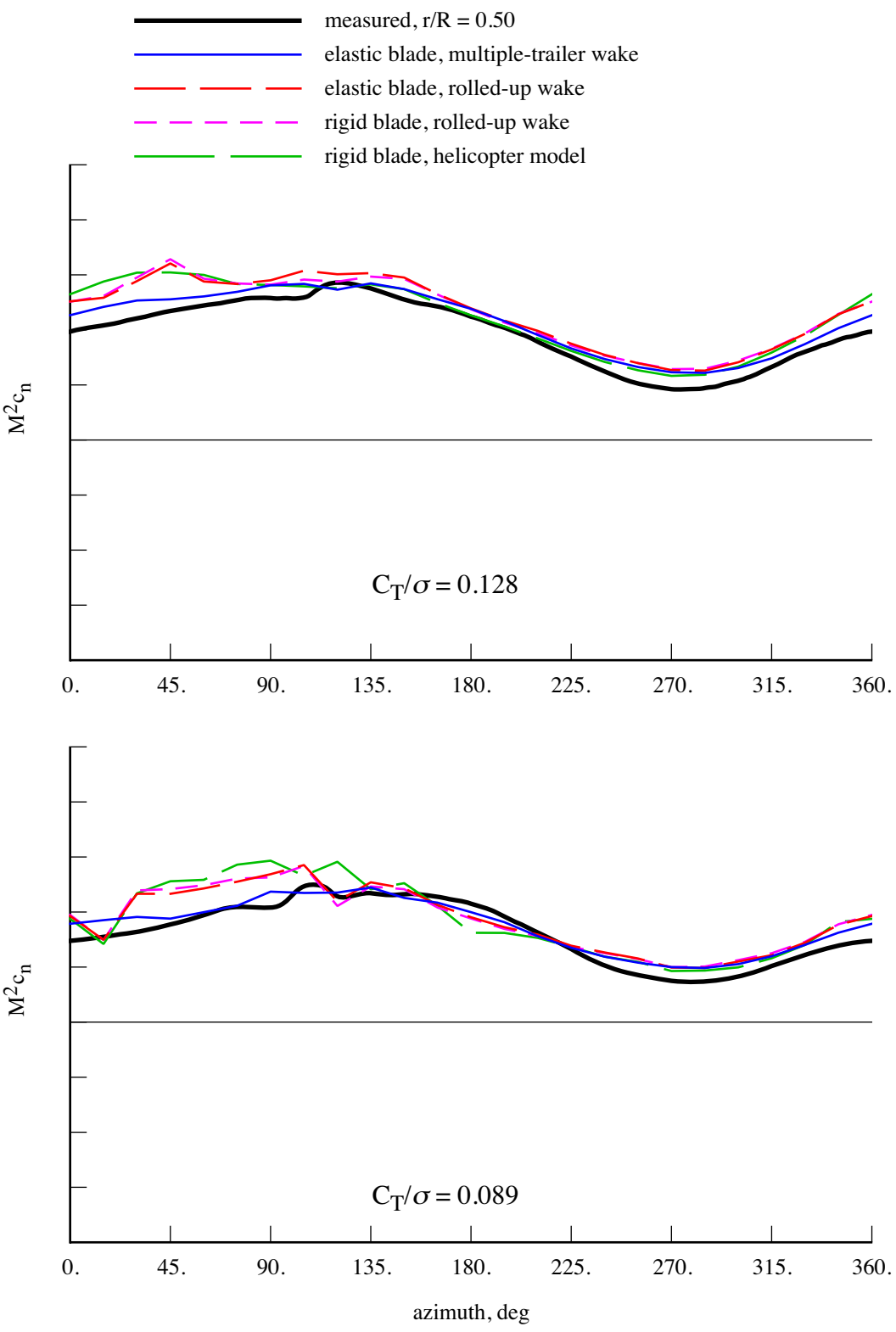

Figure 14. Measured and calculated TRAM helicopter mode airloads for μ = 0.15 and α_s = −6; radial station r = 0.50R.

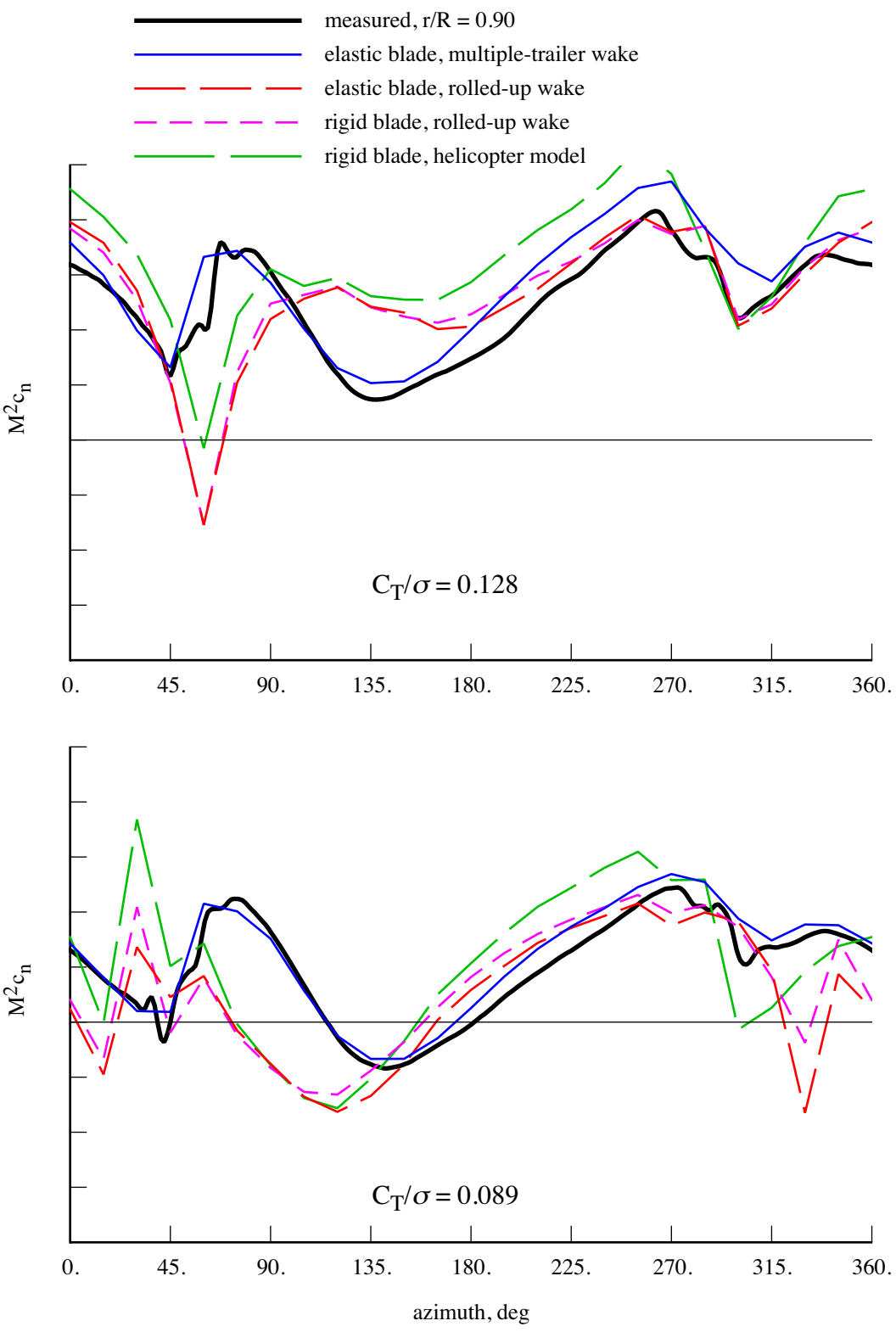

Figure 15. Measured and calculated TRAM helicopter mode airloads for μ = 0.15 and α_s = 6; radial station r = 0.90R.

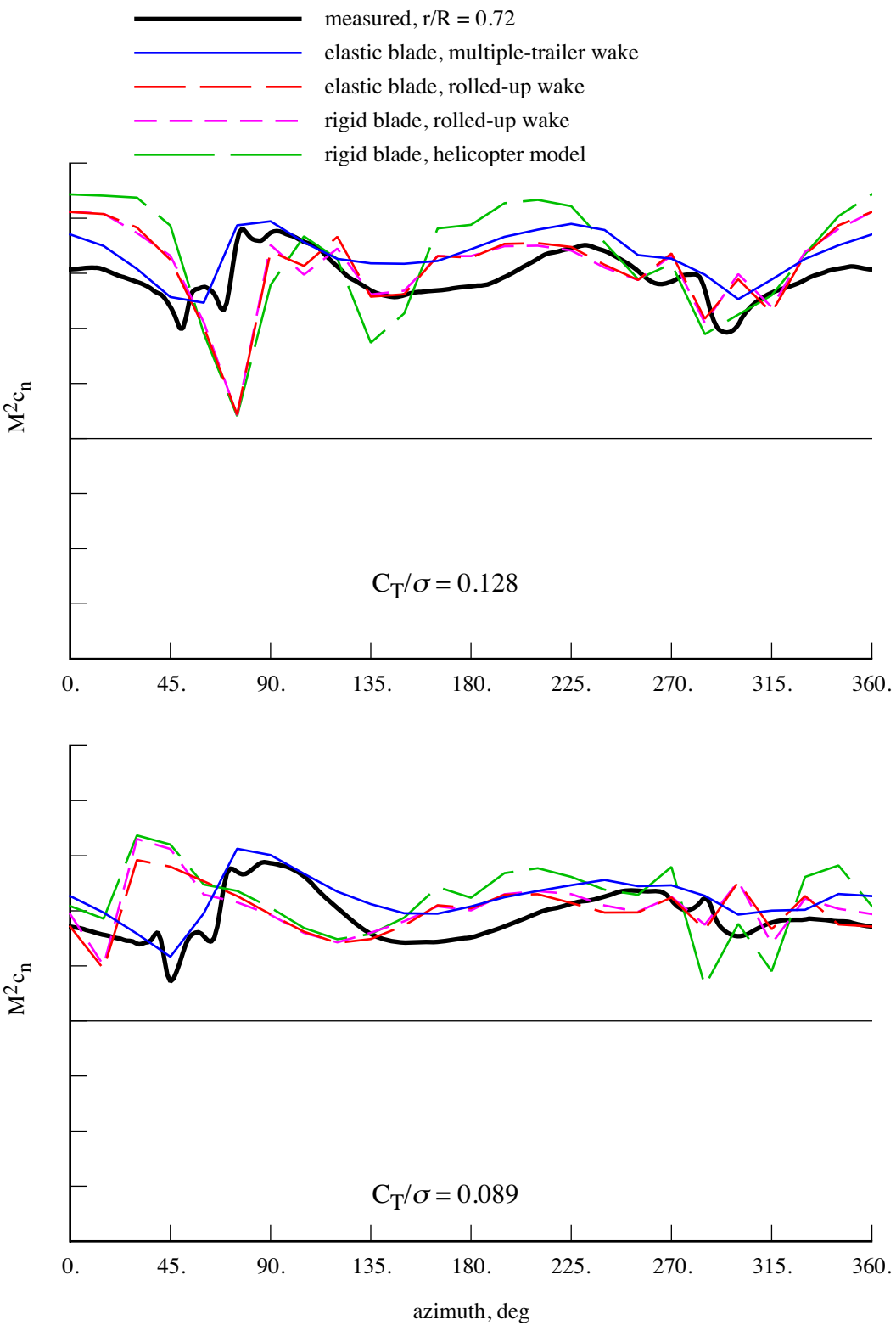

Figure 16. Measured and calculated TRAM helicopter mode airloads for μ = 0.15 and α_s = 6; radial station r = 0.72R.

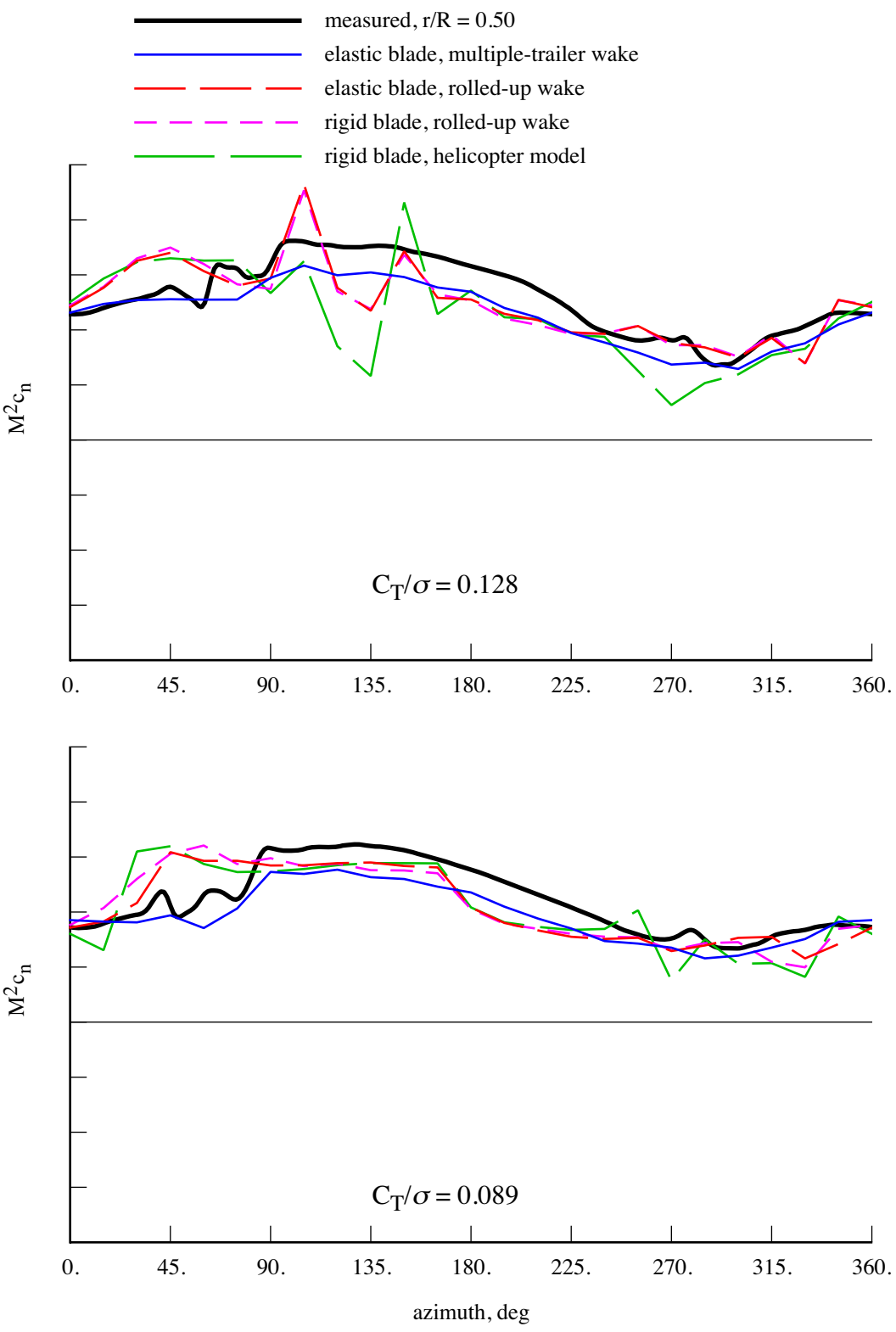

Figure 17. Measured and calculated TRAM helicopter mode airloads for μ = 0.15 and α_s = 6; radial station r = 0.50R.

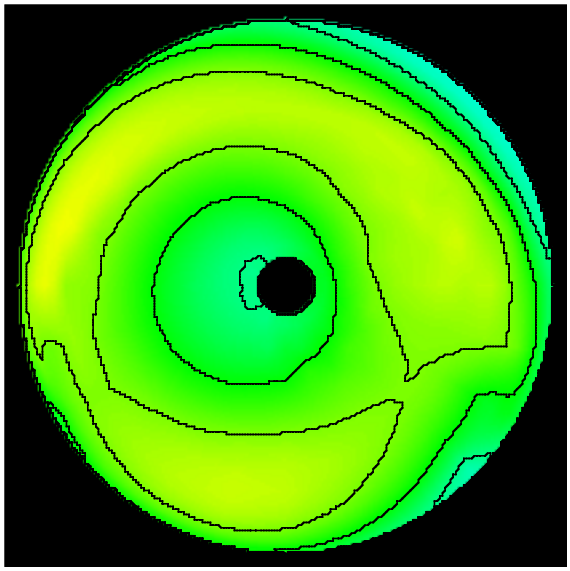

tiltrotor model, multiple-trailer wake

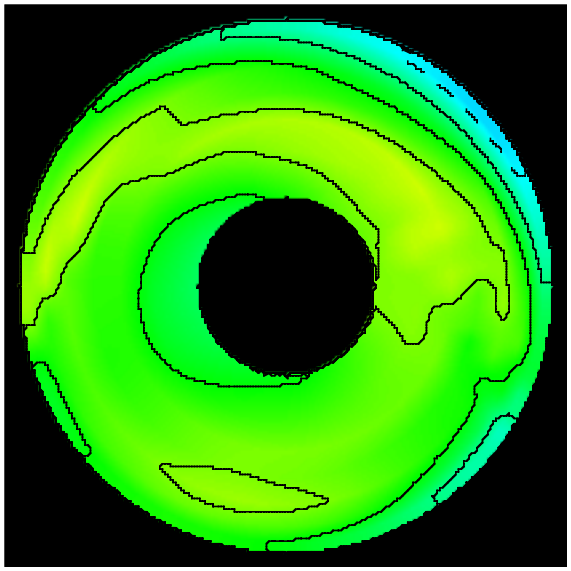

measured

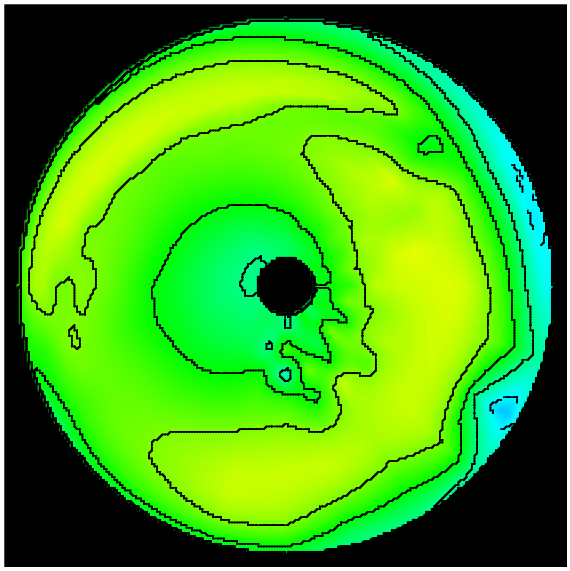

tiltrotor model, rolled-up wake

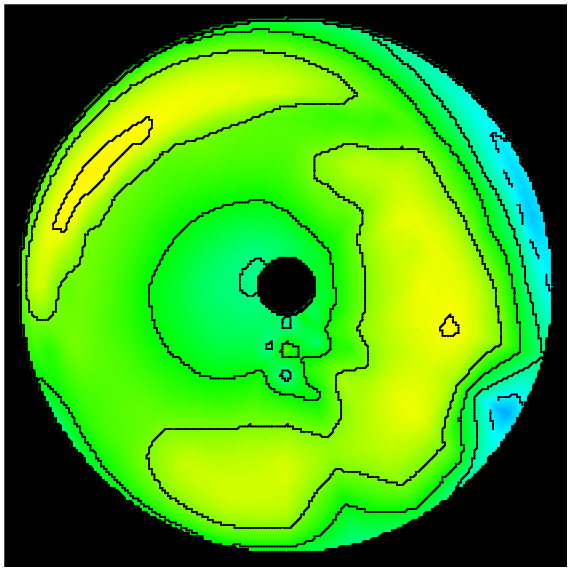

helicopter model

Figure 18. Calculated distribution of M^2c_n over rotor disk, at $\mu = 0.15$, $\alpha_s = -6$, $C_T/\sigma = 0.089$ (front of rotor disk at top, advancing side to right; dotted lines negative).

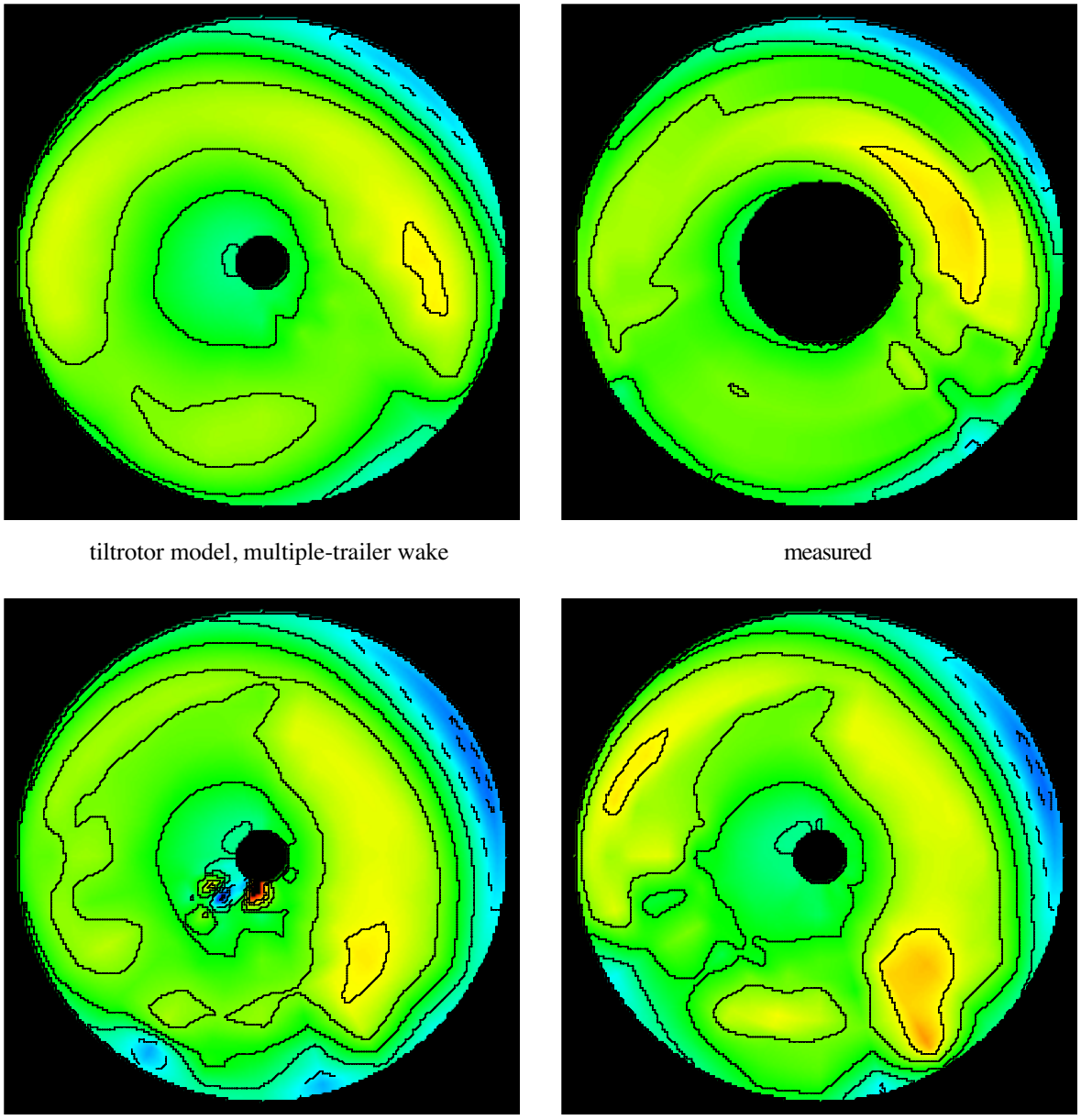

tiltrotor model, multiple-trailer wake

measured

tiltrotor model, rolled-up wake

helicopter model

Figure 19. Calculated distribution of M^2c_n over rotor disk, at $\mu = 0.15$, $\alpha_s = 6$, $C_T/\sigma = 0.089$ (front of rotor disk at top, advancing side to right; dotted lines negative).

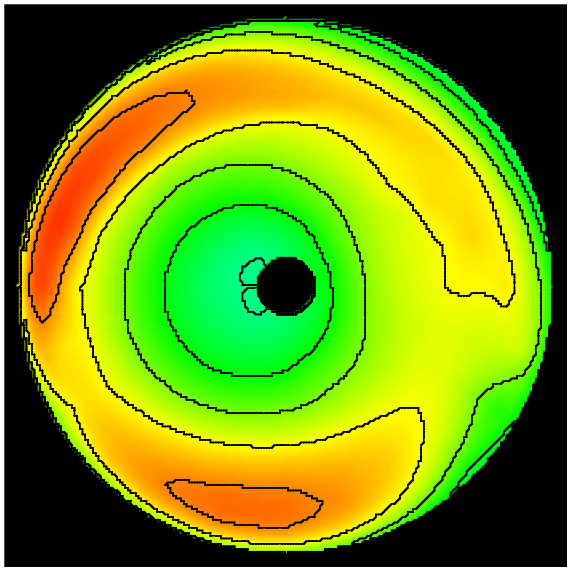

tiltrotor model, multiple-trailer wake

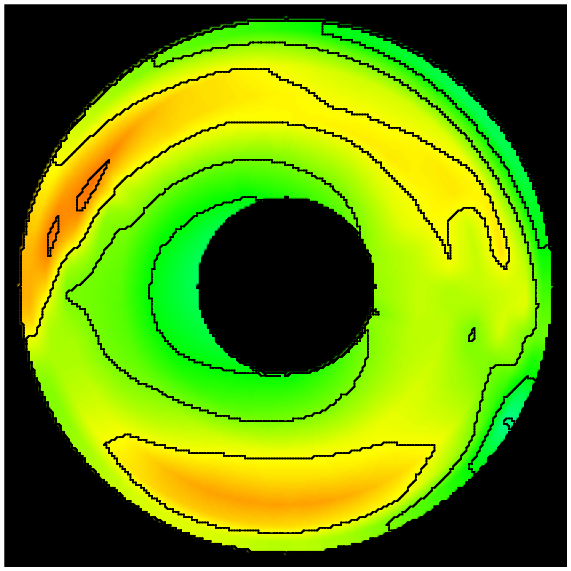

measured

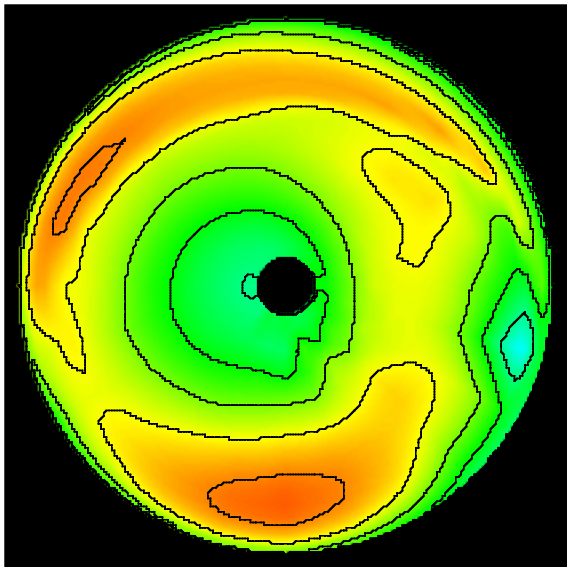

tiltrotor model, rolled-up wake

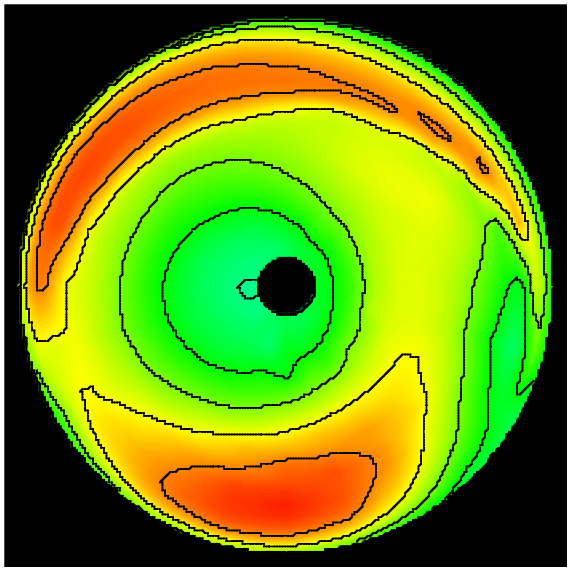

helicopter model

Figure 20. Calculated distribution of M^2c_n over rotor disk, at $\mu = 0.15$, $\alpha_s = -6$, $C_T/\sigma = 0.128$ (front of rotor disk at top, advancing side to right; dotted lines negative).

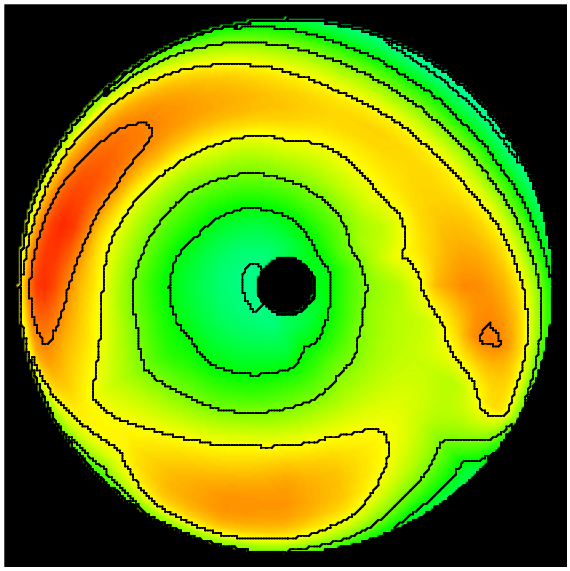

tiltrotor model, multiple-trailer wake

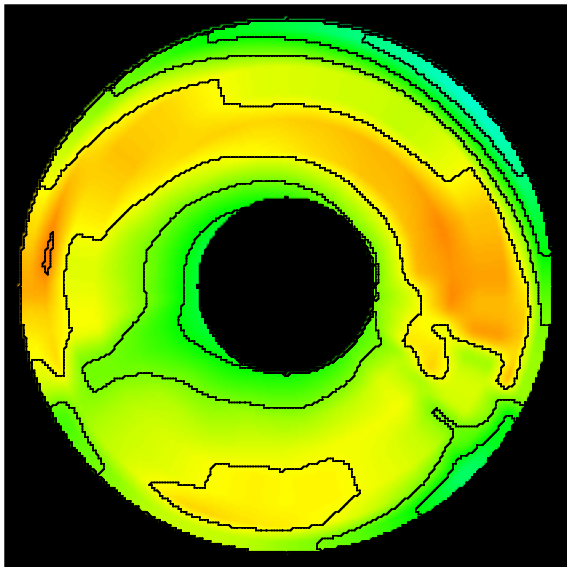

measured

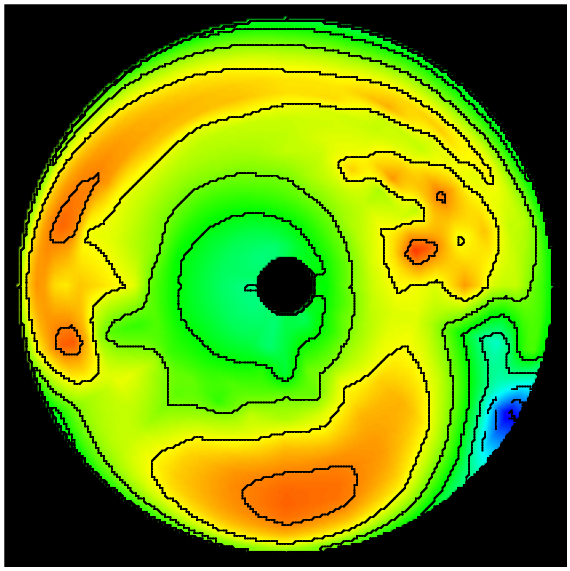

tiltrotor model, rolled-up wake

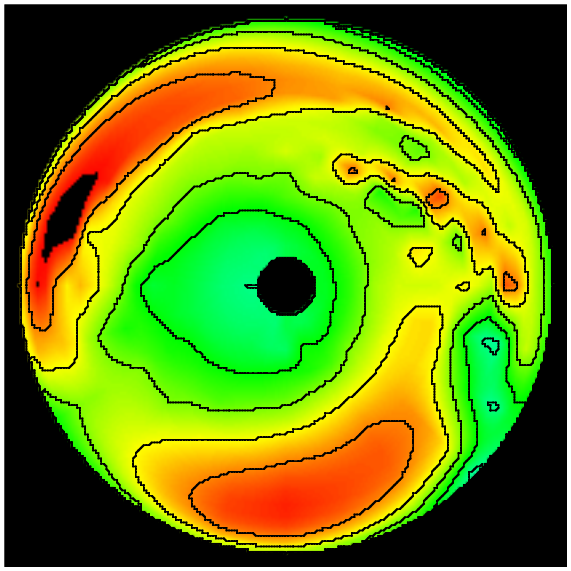

helicopter model

Figure 21. Calculated distribution of M^2c_n over rotor disk, at $\mu = 0.15$, $\alpha_s = 6$, $C_T/\sigma = 0.128$ (front of rotor disk at top, advancing side to right; dotted lines negative).

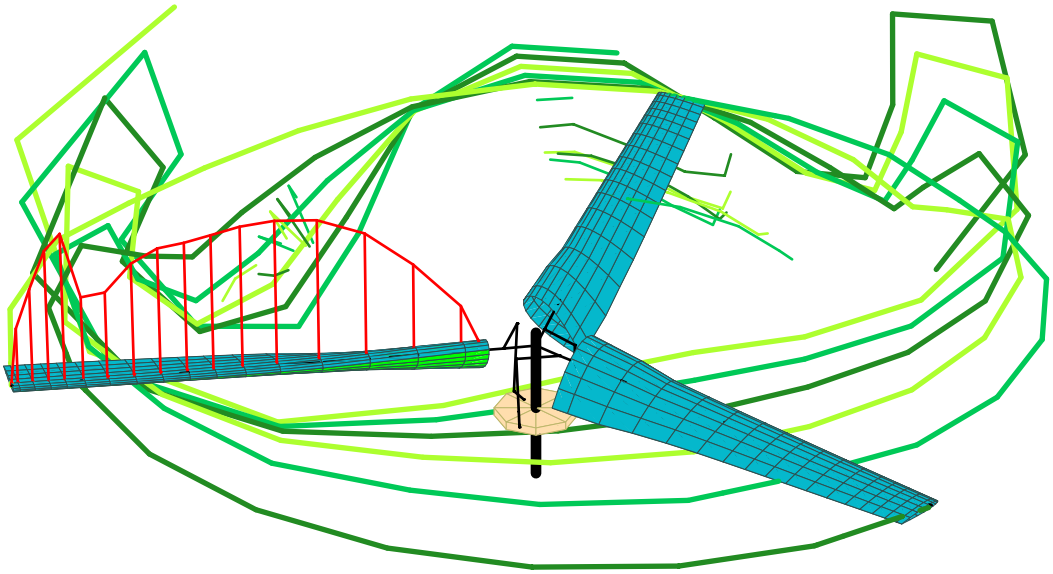

Figure 22a. Calculated TRAM wake geometry and loading for $\mu = 0.15$, $\alpha_s = -6$, $C_T/\sigma = 0.128$. Rolled-up wake model, azimuth of reference blade = 105 deg.

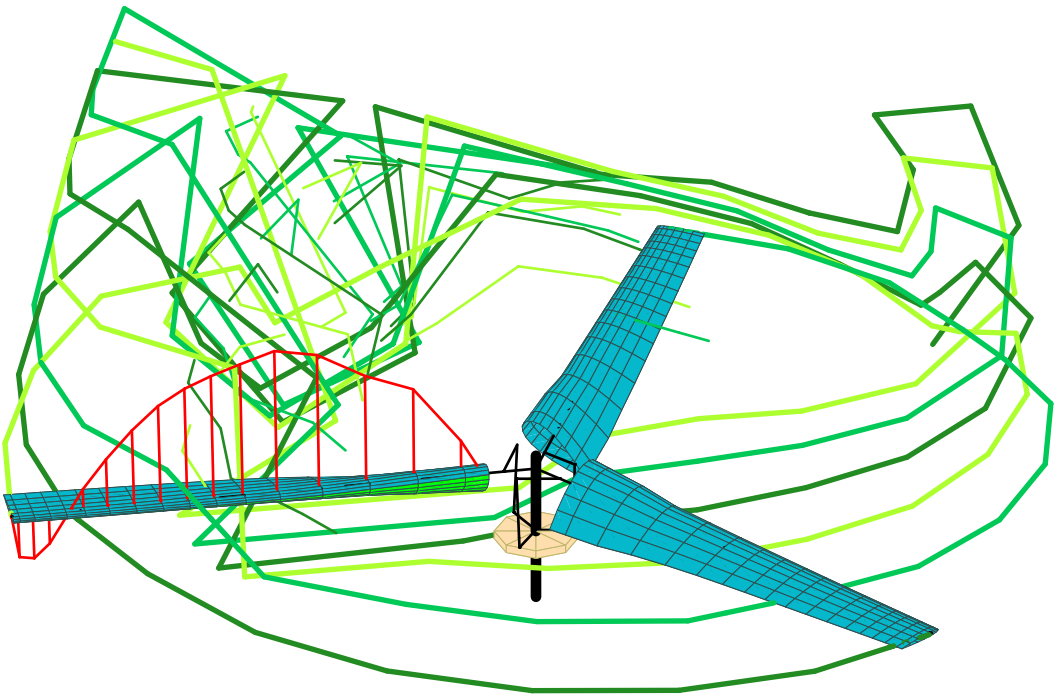

Figure 22b. Calculated TRAM wake geometry and loading for $\mu = 0.15$, $\alpha_s = -6$, $C_T/\sigma = 0.089$. Rolled-up wake model, azimuth of reference blade = 105 deg.

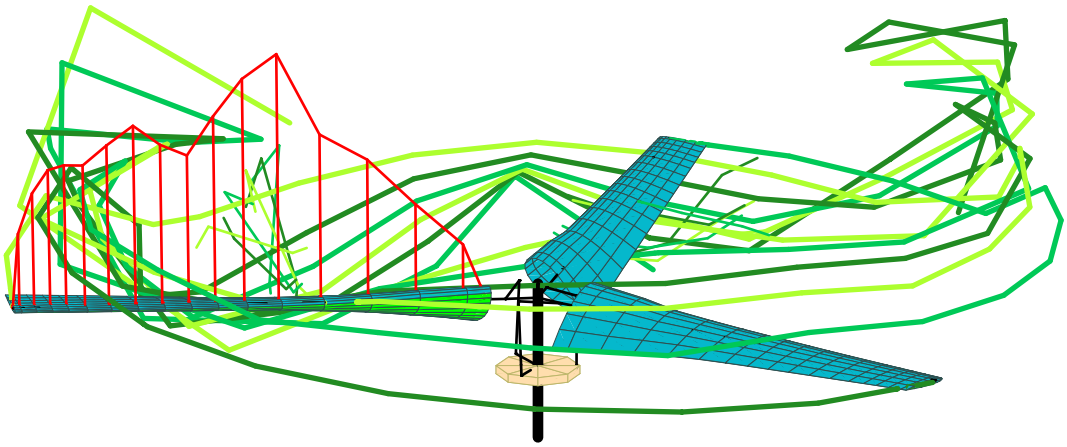

Figure 23a. Calculated TRAM wake geometry and loading for $\mu = 0.15$, $\alpha_s = 6$, $C_T/\sigma = 0.128$. Rolled-up wake model, azimuth of reference blade = 105 deg.

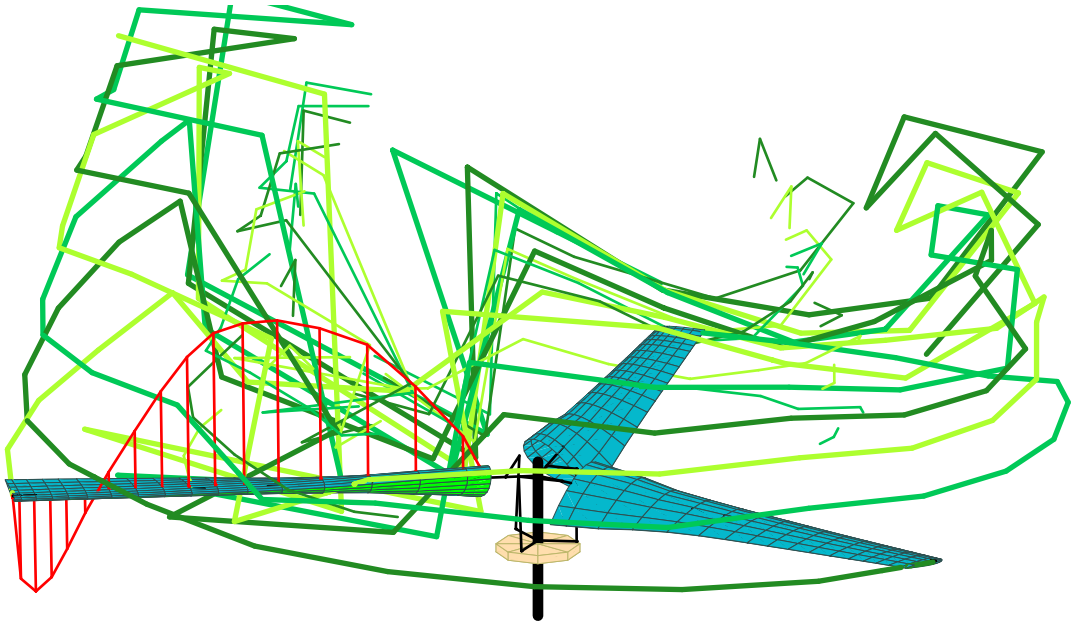

Figure 23b. Calculated TRAM wake geometry and loading for $\mu = 0.15$, $\alpha_s = 6$, $C_T/\sigma = 0.089$. Rolled-up wake model, azimuth of reference blade = 105 deg.

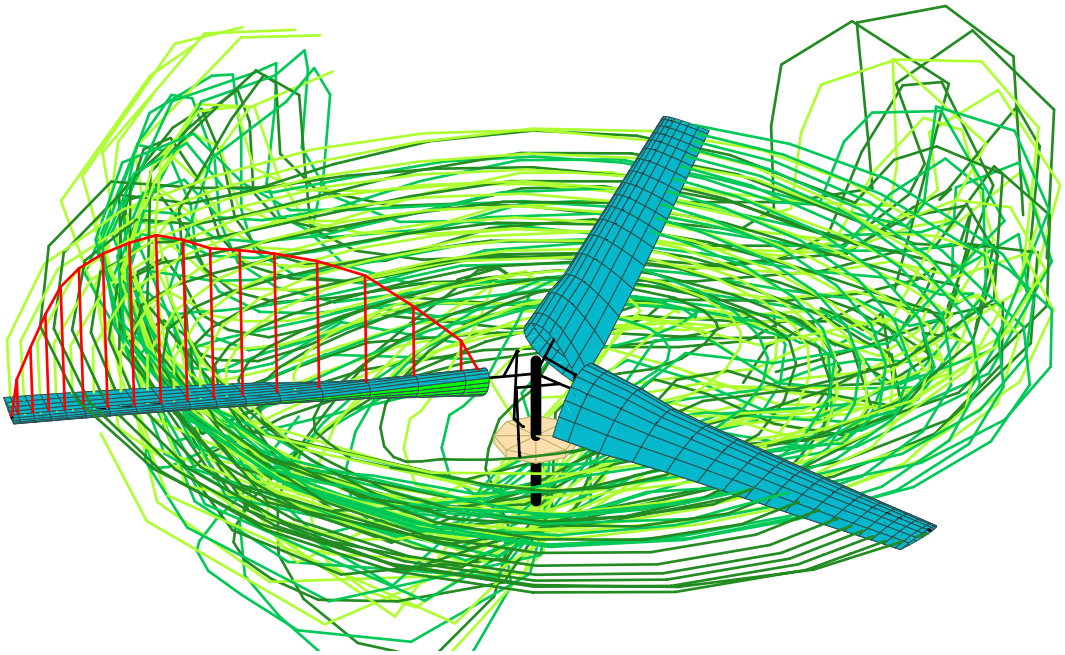

Figure 24a. Calculated TRAM wake geometry and loading for $\mu = 0.15$, $\alpha_S = -6$, $C_T/\sigma = 0.128$. Multiple-trailer wake model, azimuth of reference blade = 105 deg.

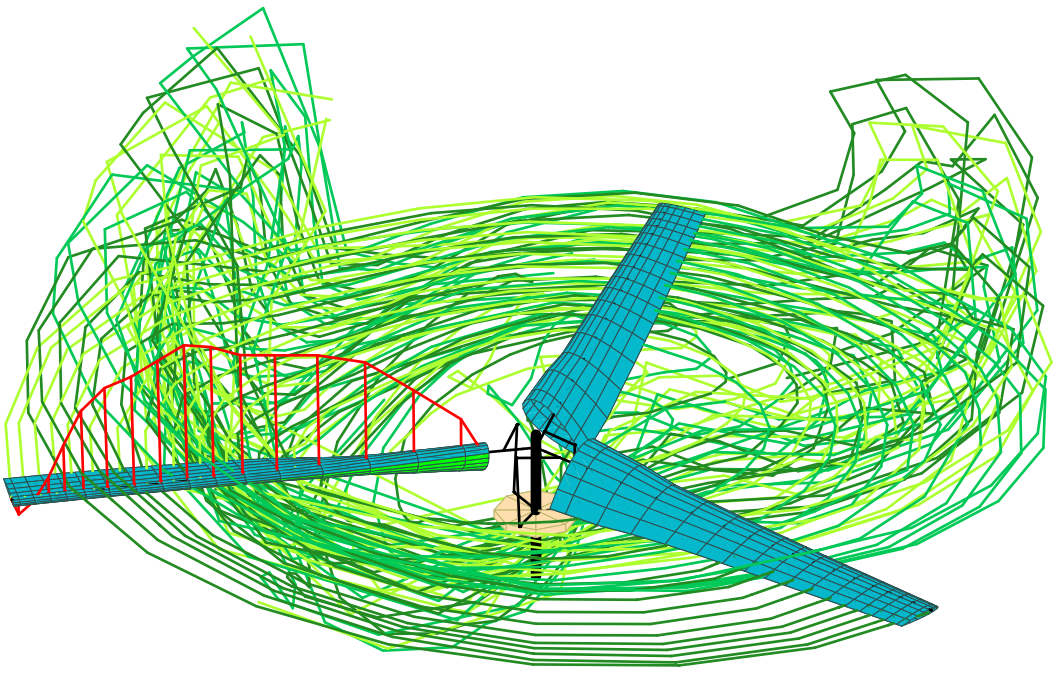

Figure 24b. Calculated TRAM wake geometry and loading for $\mu = 0.15$, $\alpha_S = -6$, $C_T/\sigma = 0.089$. Multiple-trailer wake model, azimuth of reference blade = 105 deg.

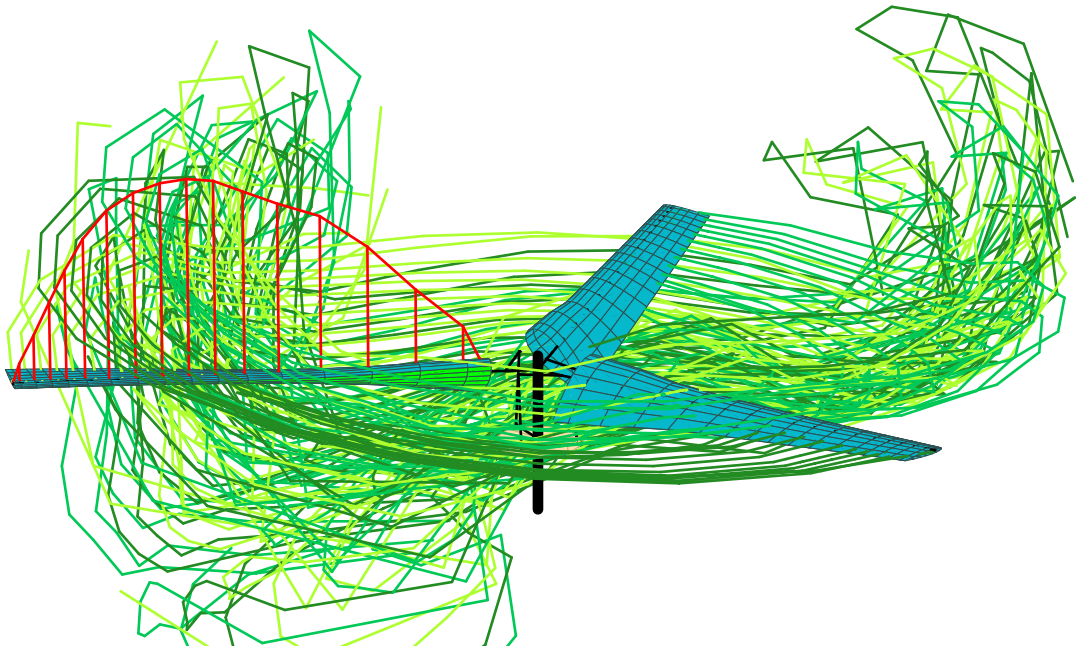

Figure 25a. Calculated TRAM wake geometry and loading for $\mu = 0.15$, $\alpha_S = 6$, $C_T/\sigma = 0.128$. Multiple-trailer wake model, azimuth of reference blade = 105 deg.

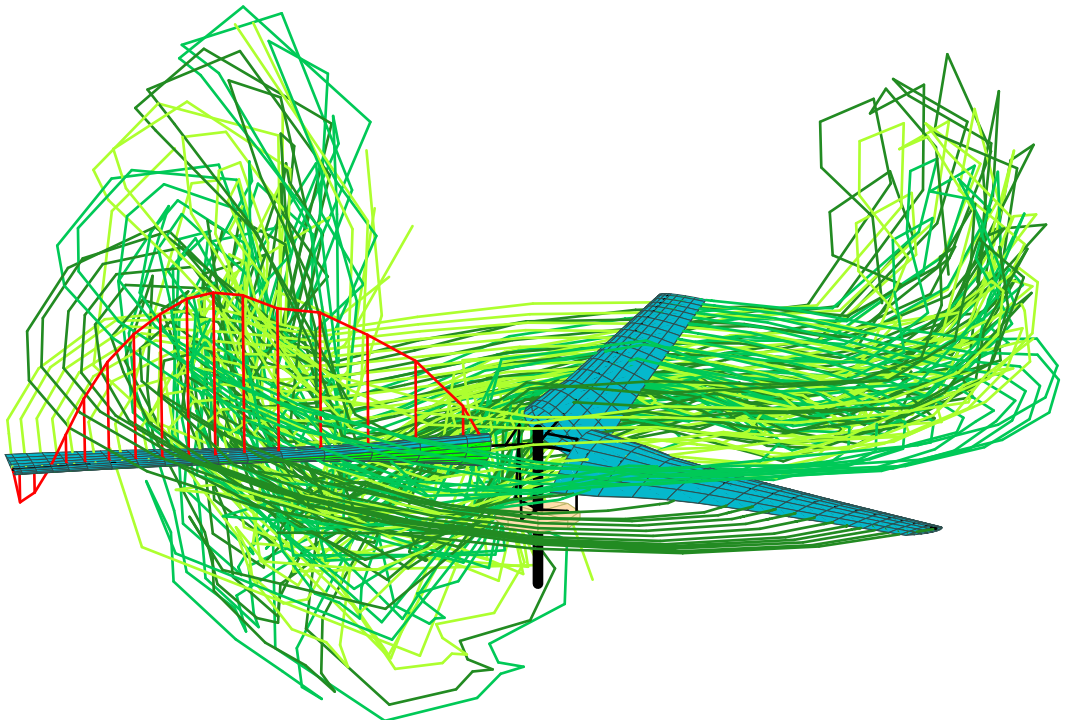

Figure 25b. Calculated TRAM wake geometry and loading for $\mu = 0.15$, $\alpha_S = 6$, $C_T/\sigma = 0.089$. Multiple-trailer wake model, azimuth of reference blade = 105 deg.

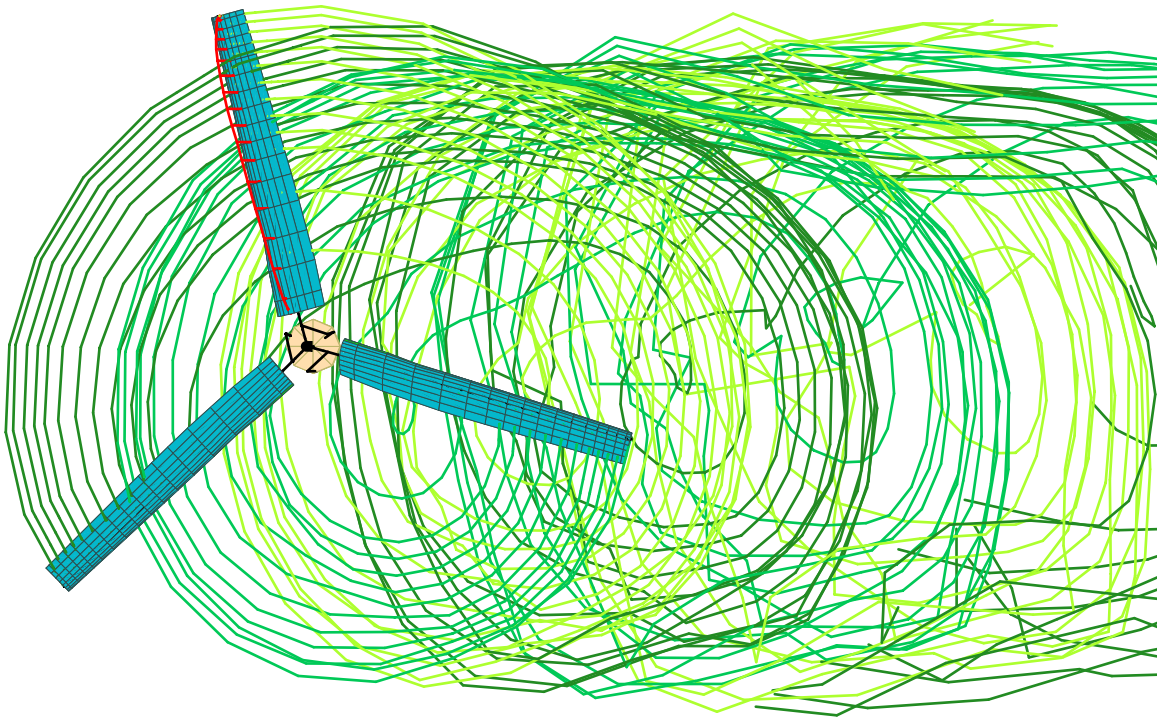

Figure 26a. Calculated TRAM wake geometry and loading for $\mu = 0.15$, $\alpha_S = -6$, $C_T/\sigma = 0.128$. Multiple-trailer wake model (top view), azimuth of reference blade = 105 deg.

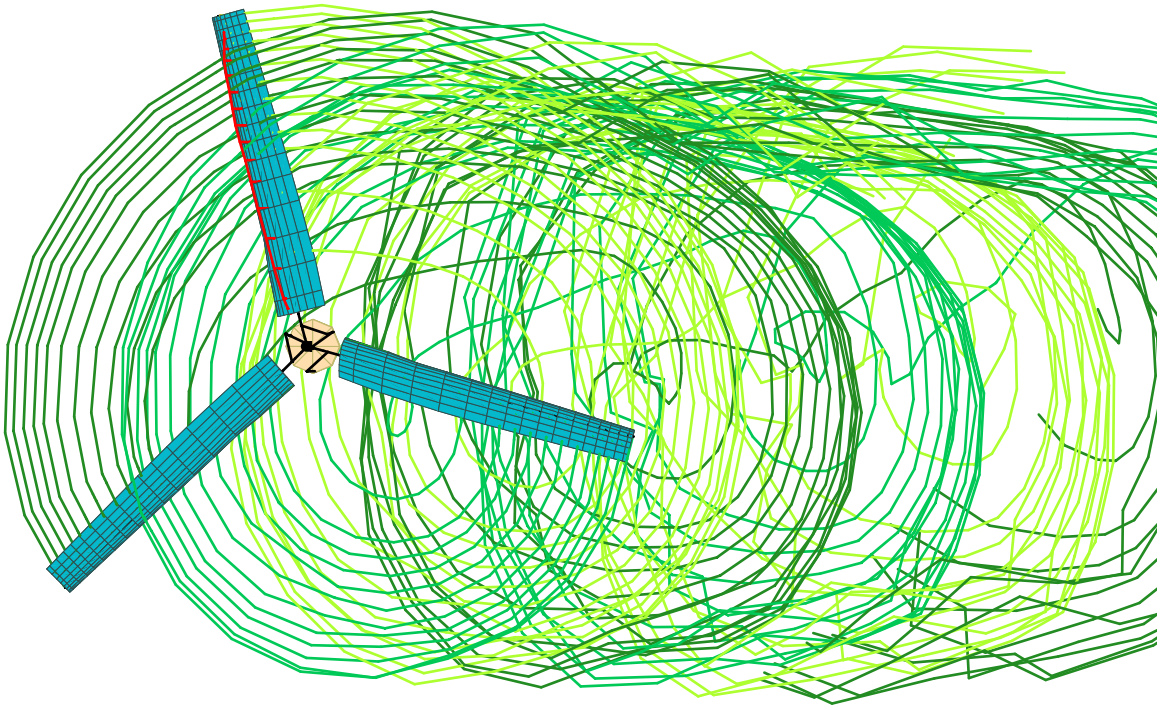

Figure 26b. Calculated TRAM wake geometry and loading for $\mu = 0.15$, $\alpha_S = -6$, $C_T/\sigma = 0.089$. Multiple-trailer wake model (top view), azimuth of reference blade = 105 deg.

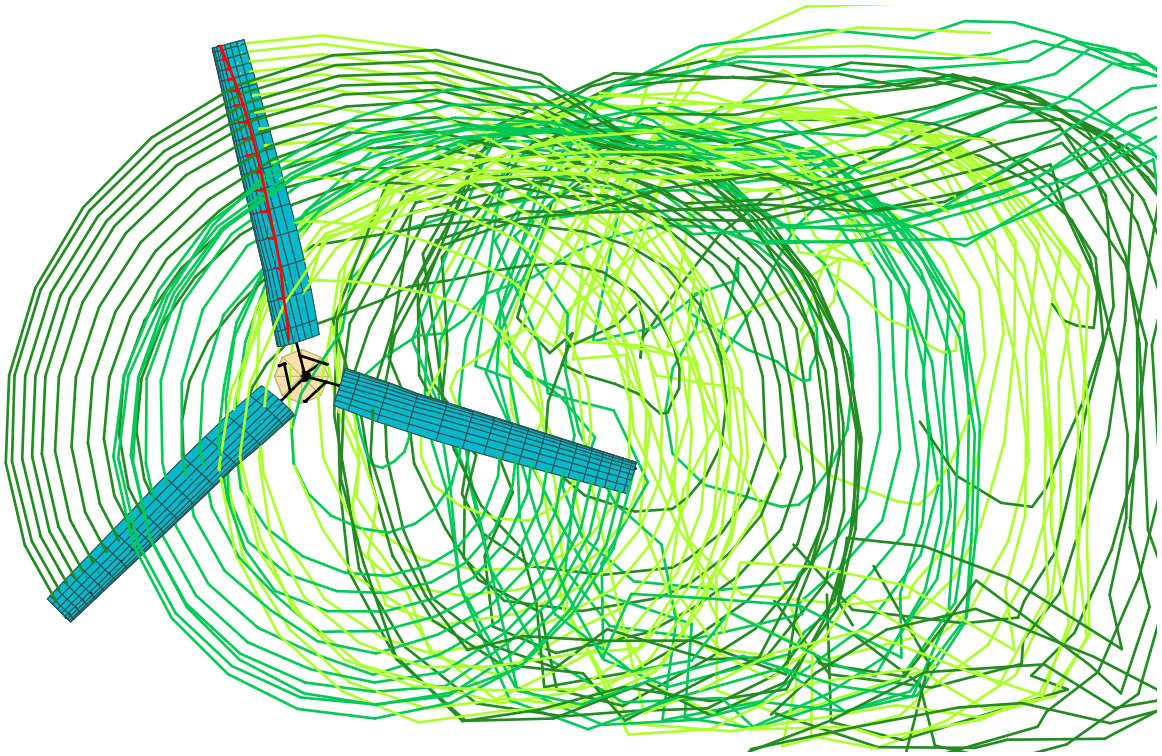

Figure 27a. Calculated TRAM wake geometry and loading for $\mu = 0.15$, $\alpha_S = 6$, $C_T/\sigma = 0.128$. Multiple-trailer wake model (top view), azimuth of reference blade = 105 deg.

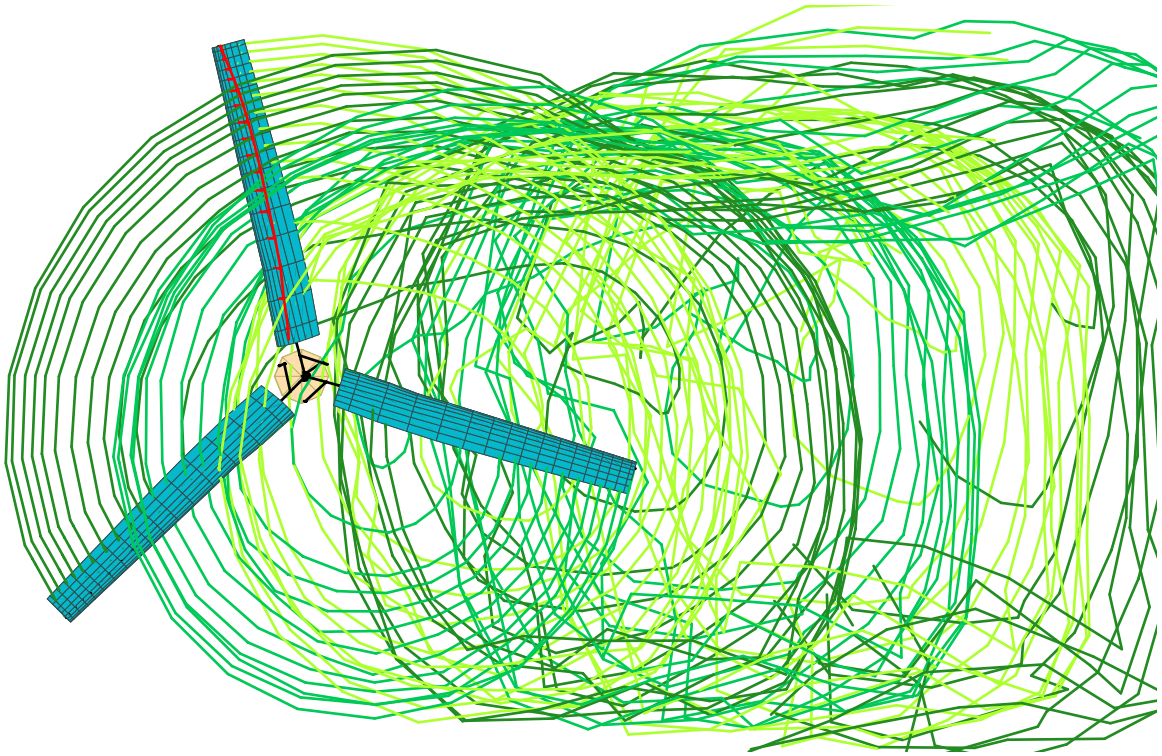

Figure 27b. Calculated TRAM wake geometry and loading for $\mu = 0.15$, $\alpha_S = 6$, $C_T/\sigma = 0.089$. Multiple-trailer wake model (top view), azimuth of reference blade = 105 deg.